PERGAMON

Deep-Sea Research I 48 (2001) 1757–1792

DEEP-SEA RESEARCH
PART I

www.elsevier.com/locate/dsr

The Arctic Ocean Boundary Current along the Eurasian slope and the adjacent Lomonosov Ridge: Water mass properties, transports and transformations from moored instruments

Rebecca A. Woodgate[a,*], Knut Aagaard[a], Robin D. Muench[b], John Gunn[b], Göran Björk[c], Bert Rudels[d], A.T. Roach[a], Ursula Schauer[e]

[a]*Polar Science Center, Applied Physics Laboratory, University of Washington, 1013 NE 40th Street, Seattle WA 98105-6698, USA*
[b]*Earth & Space Research, 1910 Fairview East, Suite 102, Seattle, WA 98102-3620, USA*
[c]*Earth Sciences Centre, Göteborg University, Box 460, SE 405 30 Göteborg, Sweden*
[d]*Finnish Institute of Marine Research, P.O. Box 33, FIN-00931, Helsinki, Finland*
[e]*Alfred-Wegener-Institute für Polar- und Meeresforschung, Columbusstrasse, 27570 Bremerhaven, Germany*

Received 14 December 1999; received in revised form 11 April 2000; accepted 25 September 2000

Abstract

Year-long (summer 1995 to 1996) time series of temperature, salinity and current velocity from three slope sites spanning the junction of the Lomonosov Ridge with the Eurasian continent are used to quantify the water properties, transformations and transport of the boundary current of the Arctic Ocean.

The mean flow is cyclonic, weak (1 to 5 cm s^{-1}), predominantly aligned along isobaths and has an equivalent barotropic structure in the vertical. We estimate the transport of the boundary current in the Eurasian Basin to be 5 ± 1 Sv. About half of this flow is diverted north along the Eurasian Basin side of the Lomonosov Ridge. The warm waters ($> 1.4°C$) of the Atlantic layer are also found on the Canadian Basin side of the ridge south of 86.5°N, but not north of this latitude. This suggests that the Atlantic layer crosses the ridge at various latitudes south of 86.5°N and flows southward along the Canadian Basin side of the ridge.

Temperature and salinity records indicate a small (0.02 Sv), episodic flow of Canadian Basin deep water into the Eurasian Basin at ~ 1700 m, providing a possible source for an anomalous eddy observed in the Amundsen Basin in 1996. There is also a similar flow of Eurasian Basin deep water into the Canadian Basin. Both flows probably pass through a gap in the Lomonosov Ridge at 80.4°N.

A cooling and freshening of the Atlantic layer, observed at all three moorings, is attributed to changes (in temperature and salinity and/or volume) in the outflow from the Barents Sea the previous winter, possibly

Regional terms: Arctic Ocean; Eurasian Basin; Canadian Basin; Lomonosov Ridge; Barents Sea

* Corresponding author. Tel.: + 1-206-221-3268; fax: + 1-206-616-3142.
E-mail address: woodgate@apl.washington.edu (R.A. Woodgate).

0967-0637/01/$ - see front matter
PII: S0967-0637(00)00091-1

caused by an observed increased flow of ice from the Arctic Ocean into the Barents Sea. The change in water properties, which advects at ~ 5 cm s^{-1} along the southern edge of the Eurasian Basin, also strengthens the cold halocline layer and increases the stability of the upper ocean. This suggests a feedback in which ice exported from the Arctic Ocean into the Barents Sea promotes ice growth elsewhere in the Arctic Ocean.

The strongest currents recorded at the moorings (up to 40 cm s^{-1}) are related to eddy features which are predominantly anticyclonic and, with a few exceptions, are of two main types: cold core eddies, confined to the upper 100–300 m, probably formed on the shelf, and warm core eddies of greater vertical extent, probably related to instabilities of an upstream front.

Keywords: Polar oceanography; Boundary current; Mass transport; Water masses; Halocline; Mesoscale eddies

1. Introduction

Present understanding of the circulation of the Arctic Ocean is largely built on a combination of hydrographic measurements and observations of ice motion. Both methodologies have a long history in the Polar Basin, beginning with measurements during the drift of the research vessel *Fram* over 100 years ago (Nansen, 1902), but both also are limited in their ability to illuminate the ocean circulation, the former most importantly because of the apparently weak baroclinic circulation (Swift et al., 1997), and the latter because the ice drift appears to be largely decoupled from the circulation below a few tens of meters (Aagaard, 1989). To a large extent, rather than being directly measured, the flow in the Arctic Ocean has been inferred from the spatial distribution of temperature, salinity and other tracers. Apart from upper-ocean boundary layer work (e.g., Hunkins, 1966; McPhee and Smith, 1976), direct velocity measurements in the Arctic Ocean are very sparse, especially measurements of any temporal extent or away from the shelves. For example, we are aware of only one earlier moored array over the Lomonosov Ridge, which during 1979 yielded three time series of velocity and temperature of 5 to 6 weeks duration (Aagaard, 1981).

We present here thirteen year-long measurements of temperature, salinity and velocity from various depths at three locations near the junction of the Lomonosov Ridge with the Eurasian continent. Two moorings (LM1 and LM3) were sited on the slope on either side of the ridge, i.e., north of the Laptev and East Siberian seas, while the third mooring (LM2) was located on the Eurasian Basin flank of the ridge some 200 km north of the shelf break (Fig. 1). Instruments were distributed through the water column, which extended to 1700 m at the three sites.

Our primary objective in making the measurements was to examine the boundary current over the slope near the intersection of the ridge and the continental margin, where the flow, which is directed eastward along the shelf break (past LM1), is believed to partition into separate streams, one following the ridge northward (past LM2) and across the Arctic Ocean, and the other continuing along the continental slope (past LM3) into the Canadian Basin (Aagaard, 1989; Rudels et al., 1994; McLaughlin et al., 1996).

Together with hydrographic sections run during the deployment and recovery cruises, the moored time series proved particularly useful in illuminating five issues, which provide our focus in this paper: (1) exchanges of deep water between the Eurasian and Canadian basins; (2) shelf-induced changes in the Atlantic layer and the halocline; (3) circulation of the Atlantic layer near the Lomonosov Ridge; (4) vertical structure and transport in the boundary current; and (5) mesoscale

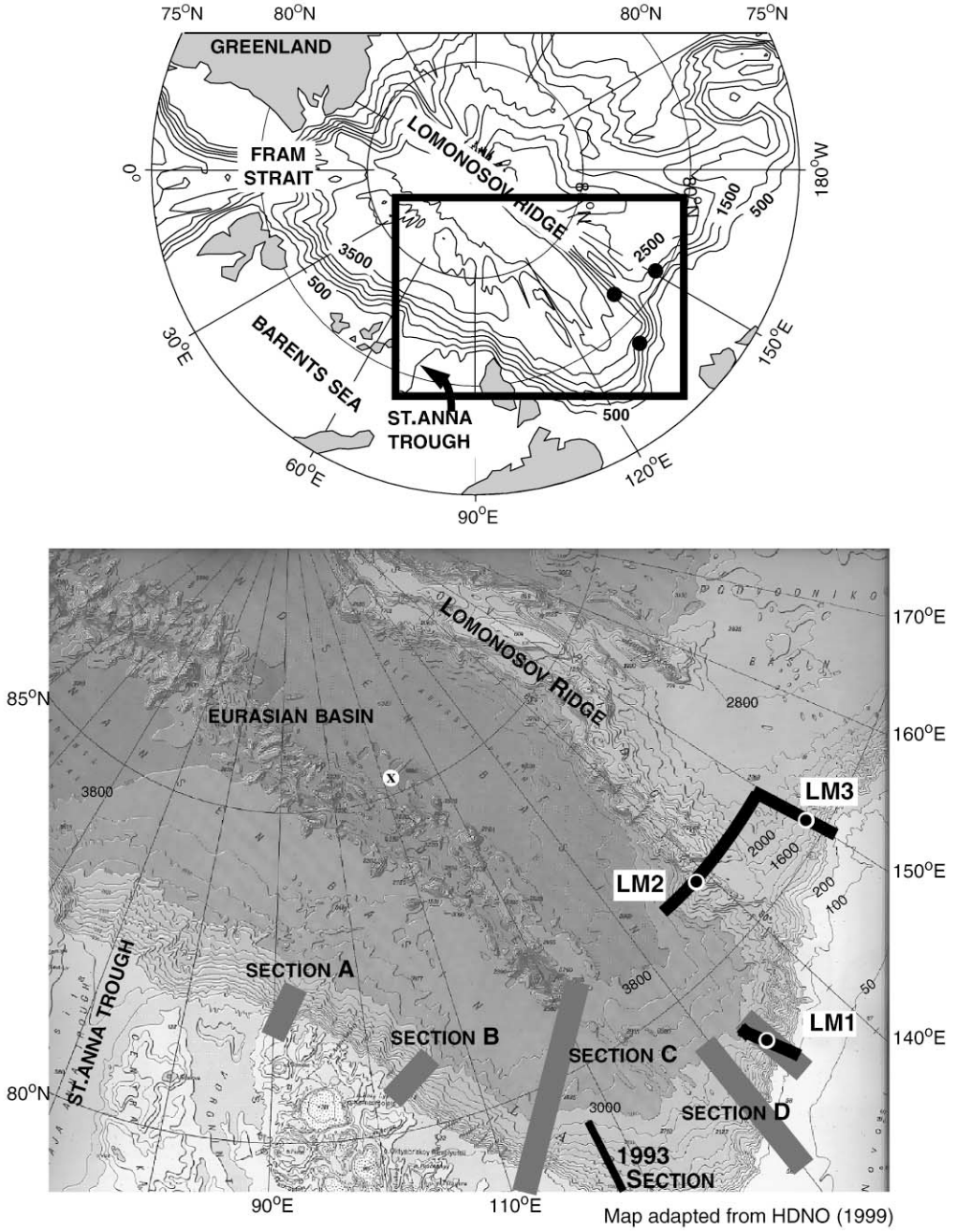

Fig. 1. Map of the Arctic Ocean, with an expanded section from the eastern Eurasian Basin. Dots mark mooring positions. On the lower plot, thick grey lines mark the Polarstern 1995 CTD sections of Fig. 11, and the thin black line, the Polarstern 1993 CTD section of Fig. 9, which extends off the map. The black lines through LM1, LM2 and LM3 mark the projected sections plotted in Appendix C. A cross marks the position of the eddy of CBDW (see Section 3.1). The topography is adapted from HDNO (1999).

features, especially eddies. Item (2) is of particular interest in the context of recent large changes in the stratification of the upper Arctic Ocean (Steele and Boyd, 1998), while the other four have application to the transport of heat and materials within the Arctic Ocean.

2. The data

2.1. Technical description

The three moorings, LM1, LM2, LM3, (Fig. 1), were deployed between August 1995 and August 1996, and carried thirteen Aanderaa Recording Current Meters (RCMs) and nine Seabird Seacats (SBEs). The instrument depths (Table 1) were designed to sample the lower halocline ($\sim$ 100 m

Table 1
Summary of mooring statistics for unfiltered data[a]

ID	Position, latitude (N) and longitude (E)	Water depth (m)	Instrument depth (m)	Instrument type	Extent of record (days)	Mean velocity magnitude & direction (cm s^{-1} and deg)		Eddy kinetic energy (g cm^{-1} s^{-2})
LM1	78°30.8′	1761	106	RCM	382	6.1	45	31
	133°57.7′		107	SBE	382			
			326	RCM	382	5.4	39	15
			327	SBE	382			
			761	RCM	382	4.6	39	11
			1161	RCM	382	3.4	40	7
			1743	SBE	382			
LM2	81°4.5′	1712	112	RCM	365	2.1	3	29
	138°54.0′		113	SBE	365			
			272	RCM	365	1.3	4	25
			273	SBE	365			
			712	RCM	365	1.1	6	9
			1112	RCM	365	0.9	20	3
			1692	RCM	365	2.4	13	7
			1693	SBE	365			
LM3	80°19.2′	1699	99	RCM	366	2.2	82	14
	150°3.5′		100	SBE	204			
			269	RCM	366	2.7	87	11
			270	SBE	366			
			709	RCM	366	2.2	77	5
			1109	RCM	366	1.4	86	3
			1679	SBE	366			

[a]RCM = Recording Current Meter, measuring velocity and temperature. SBE = Seacat instrument, measuring temperature and conductivity (and hence salinity).

deep), the Atlantic core ($\sim$ 300 m), the mid water column ($\sim$700 and 1100 m) and the near-bottom layer ($\sim$1700 m). All instruments were calibrated before and after deployment. The SBEs recorded temperature and conductivity (thus yielding salinity) every 30 minutes, with an accuracy of 0.02°C and 0.0012 S m^{-1} (equivalent to a salinity change of 0.02 psu[1]) over the year-long deployment. The SBE records agree well with CTD casts taken before the mooring deployment and after the mooring recovery. The RCMs recorded current speed and direction hourly, with an estimated accuracy of 1 cm s^{-1} in speed and 5° in direction. Where stated (i.e., in Fig. 2 and the EOF analysis of Section 3.4), the data have been filtered to remove the tidal and inertial signals by using a Lanczos square-taper low-pass filter with a cut-off period of 40 hours and resampling at 6 hour intervals.

The data quality is generally good, although data from RCM 9194, placed at $\sim$ 300 m on LM2, showed a 16° dead zone in the compass direction, probably related to the compass needle jamming. Since for the rest of the record, the directions correlated well (correlation coefficient $\sim$ 0.85) with those of the underlying meter, erroneous directions on RCM 9194 were corrected to match those of the underlying meter. Although this correction affected 36% of the data, the correction was always less than 16°.

The analysis of the moored time series also draws on CTD data from the deployment cruise (Polarstern ARK11 in summer 1995, e.g., Rudels et al., 2000b) and the recovery cruise (Polarstern ARK12 in summer 1996, e.g., Augstein et al., 1997). For ease of reference, some of these CTD sections are shown in Appendix C.

2.2. General description

Stickplots (Fig. 2) illustrate the different characteristics of the flow at the three sites. The flow is strongest and least meandering at LM1 (see Table 1 for record-length statistics), with a mean flow of 6 cm s^{-1} at 100 m, decreasing to 3 cm s^{-1} at the lowest instrument (1100 m depth). The strongest currents are almost 40 cm s^{-1} at 100 m and almost 20 cm s^{-1} at depth. The flow is self-similar, i.e., equivalent barotropic (Killworth, 1992), in the vertical (see also Section 3.4). Although eddy events (Section 3.5) can reverse the flow throughout the water column, the dominant character is of an unidirectional current, with both the mean flow and the principal components aligned along isobaths, as determined from the topography of HDNO (1999).

The flow at LM2, both in the mean and in the principal components, is also along isobaths, although only about one-third the strength of that at LM1 (mean velocity at LM2 at 100 m is 2 cm s^{-1} and that at 1100 m is 1 cm s^{-1}). Thus, eddy features, which have similar strengths to those at LM1 (i.e., at LM2 nearly 30 cm s^{-1} at the top meter and about 10 cm s^{-1} at the lower meters) dominate the time series at LM2. The flow is again self-similar in the vertical. In addition, an extra RCM placed $\sim$ 20 m above the bottom shows the flow to be bottom intensified, the annual mean velocity being 2.4 $\pm$ 0.1 cm s^{-1} at 1692 m compared to 1.0 $\pm$ 0.2 cm s^{-1} at 1112 m.[2] Many of the

[1] Throughout the paper, all temperatures are in situ (except for the CTD sections in Appendix C) and all salinities are measured on the Practical Salinity Scale.

[2] Errors are estimated from the variance of the velocity components and the effective number of degrees of freedom, inferred from the integral timescale.

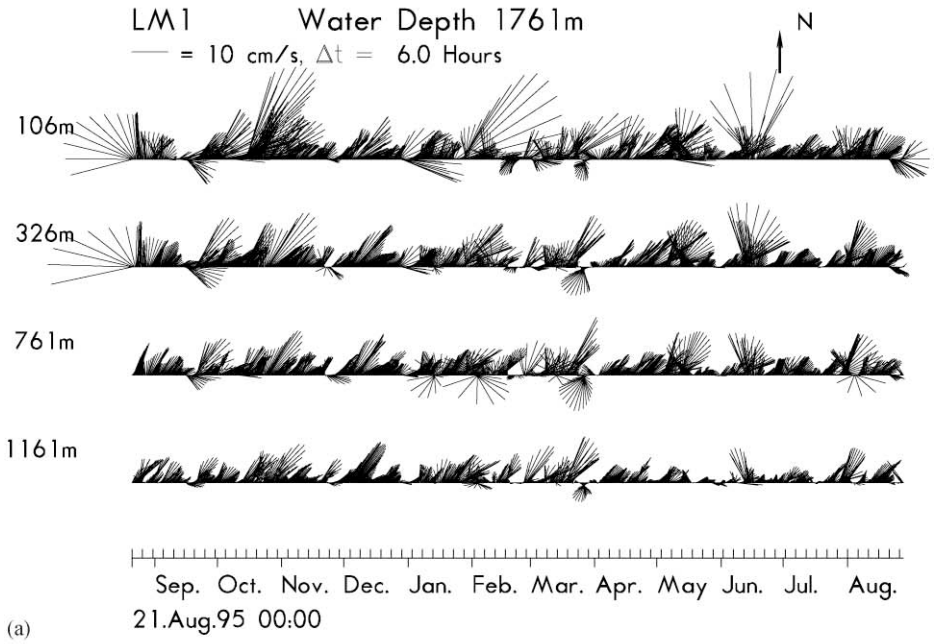

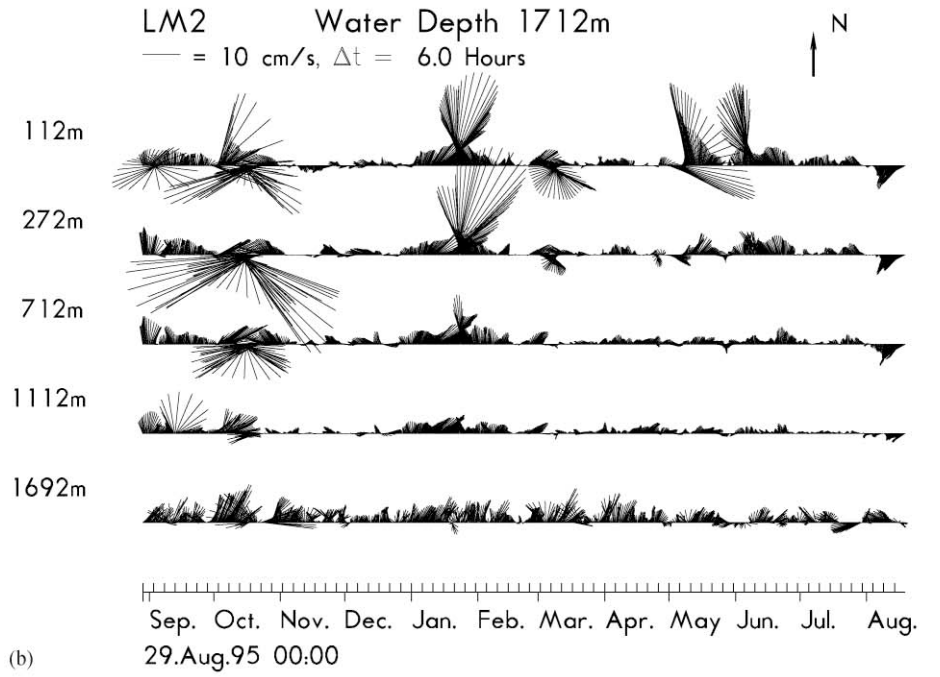

Fig. 2. Stickplots for filtered velocity from the 4 or 5 current meters on each mooring (a) LM1, (b) LM2 and (c) LM3. The length and direction of each stick gives the magnitude and direction of the 6 hour average of the filtered current.

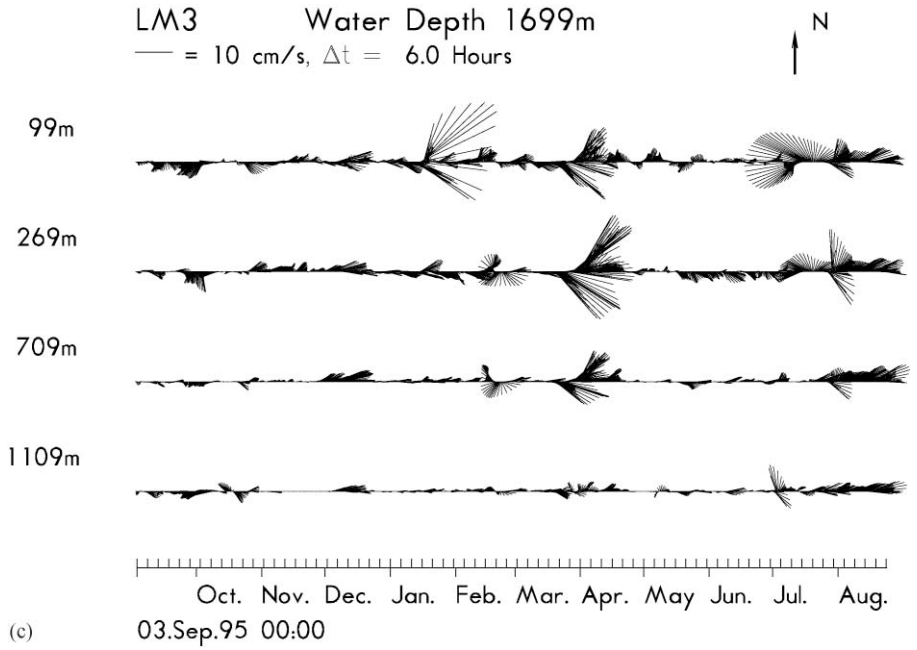

Fig. 2. (*continued*).

same features are seen at LM3, e.g., the mean flow and the principal components aligned along isobaths, the equivalent barotropic structure and the dominance of eddies. The mean flow at LM3 is almost the same strength as at LM2.

At all sites, the tidal signal is small (always less than $3\,\mathrm{cm\,s^{-1}}$, generally less than $1\,\mathrm{cm\,s^{-1}}$) and not relevant to our discussion below. However, for completeness, a tidal analysis is given in Appendix A.

Common to all three sites is the absence of an annual cycle, either in speed, direction, temperature or salinity. The wind field (obtained from NCAR/NCEP reanalysis data) near LM1 and at similar latitudes over the Eurasian Basin and the Barents Sea does show some evidence of a seasonal cycle, with winds being weakest in summer and stronger in autumn and spring. The magnitude of this seasonal cycle, however, reduces almost to zero at higher latitudes, probably due to the isolating effect of the atmospheric boundary layer (Overland and Colony, 1994). Thus, the absence of an annual cycle in our data cannot conclusively rule out wind as a dominant forcing of the boundary current. We do not, however, find any clear response in the moored data to events in the local wind field which suggests that the driving force of the current is not the local wind field. Other possible forcings include a thermohaline mechanism, which could act on a longer timescale, consistent with the record-length trends and changes which are seen in the temperature and salinity records and discussed below; or some form of eddy-topography interaction, e.g., Holloway, 1987.

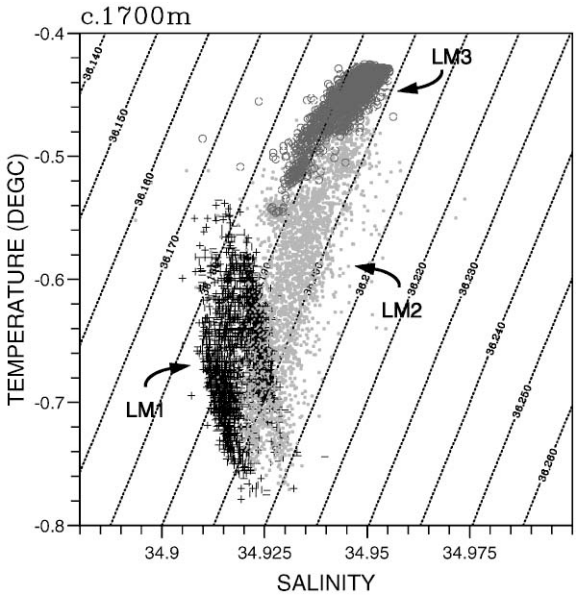

Fig. 3. Scatterplots of in situ temperature against salinity for the instruments at ~ 1700 m on LM1 (black crosses), LM2 (light grey filled dots) and LM3 (dark grey open circles). Dotted lines are isopycnals referenced to 1731 db, the average pressure of the three instruments.

3. Time series of temperature, salinity and velocity

3.1. Deep layer — exchanges between the Eurasian and Canadian basins

The deep waters of the Arctic Ocean can be divided into two categories, Eurasian Basin deep water (EBDW) and Canadian Basin deep water (CBDW), according to their temperature and salinity (T–S) (Aagaard et al., 1985). In both water masses, the salinity increases with depth. The EBDW is colder and fresher, with (in situ[3]) temperature decreasing with increasing depth and salinity, i.e., a negative gradient on a T–S plot. The CBDW is warmer and more saline, with (in situ) temperature increasing with increasing depth and salinity, i.e., a positive gradient on a T–S plot. Geographically, the two water masses are separated by the Lomonosov Ridge. Indeed, the difference in T–S properties was early evidence for the existence of the ridge (Worthington, 1953). Thus, one would expect the deepest instruments on LM1 and LM2 to measure EBDW and that on LM3 to measure CBDW.

Fig. 3 shows the year-long scatterplots of temperature and salinity for the deepest SBEs (placed ~ 20 m above the bottom) at the three mooring sites. The two forms of deep water are evident in LM1 (EBDW) and LM3 (CBDW). The properties of the water at LM2, however, coincide with an in situ isopycnal mixing line between the EBDW and the CBDW, and show a T–S range not

[3] Comparisons between different locations are made at similar depths, thus in situ temperatures are used since they give a better estimate of local temperature gradients.

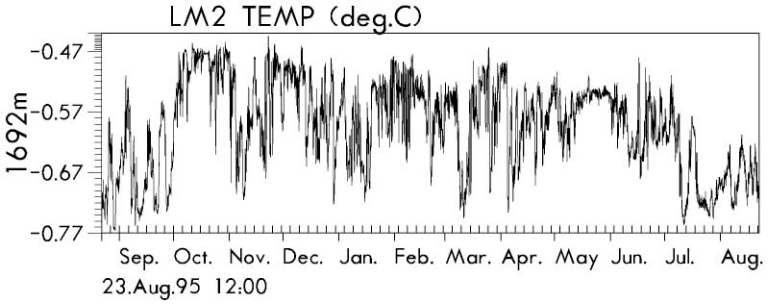

Fig. 4. Time series of in situ temperature at a depth of 1692 m (20 m above the bottom) at LM2.

previously reported from the Arctic Ocean. The time series of LM2 temperature (Fig. 4) shows large (0.2°C), rapid (occurring over $\sim$ 8 hours) jumps throughout. The coldest water, showing the least Canadian Basin influence, is found in the late summer (August and September). The warmest water, showing the most Canadian Basin influence, is found in October, concurrent with the passage of a strong ($\sim 30\,\mathrm{cm\,s^{-1}}$ at $\sim$ 300 m), warm and saline anticyclonic eddy (see Section 3.5), which extends from 100 m to at least 1100 m.

The T–S properties at LM2 suggest an episodic mixing of EBDW and CBDW. The ratio of the mixture varies, but on the yearly average it is about 1 : 1. The flow at LM2 is almost without exception northward, indicating that the CBDW must have come through the Lomonosov Ridge south of LM2. The most recent topographic chart (HDNO, 1999) shows a gap in the ridge near 80.4°N (Fig. 1), about 1700 m deep and 16 km wide, i.e., wider than the first baroclinic Rossby radius which is $\sim$ 7 km. This gap, (which is also present in the older Perry and Fleming (1986) chart), would be a possible pathway for the CBDW to enter the Eurasian Basin. The time series from LM2 of temperature (Fig. 4); the stickplot of velocity (Fig. 2b), which shows eddying or meandering features, and the scarcity of the CBDW in CTD casts taken in the area of LM2 (it is found in only two CTD casts from the deployment section, and, greatly diluted, in two CTD casts from the recovery section), all suggest that the outflow is intermittent. Using the CTD casts taken prior to the deployment of LM2 (Fig. 5) to estimate the vertical extent of the CBDW ($\sim$ 100 m); the CTD section taken across the slope at the location of LM2 to estimate the possible lateral extent ($\sim$ 20 km), and the time series data to estimate the velocity ($\sim 2\,\mathrm{cm\,s^{-1}}$), we obtain a total northward CBDW transport of order 0.02 Sv. Although this is small, corresponding to a renewal rate for the deep waters of several thousand years, it demonstrates there is a deep water outflow from the Canadian Basin.

The absence of CBDW at LM1 suggests the outflow from the gap moves northward with the Lomonosov Ridge on its right, until it is either further mixed or is dispersed into the interior in deep eddies. For example, a very similar water mass, though of far greater vertical extent (the anomaly spans 1500 m of the water column), is found at a single station in the middle of the Amundsen Basin in 1996 (Figs. 1 and 5). The oxygen minimum observed in this anomalous water mass (Augstein et al., 1997) is consistent with a Canadian Basin source. This is probably an eddy, whose volume can be estimated as between $2\times10^{11}\,\mathrm{m^3}$ and $9\times10^{11}\,\mathrm{m^3}$ by using the first baroclinic Rossby radius ($\sim$ 7 km) or the station spacing ($\sim$ 20 km) as an estimate of the eddy radius. Thus, the observed CBDW outflow could account for 1 to 5 such eddies in a year.

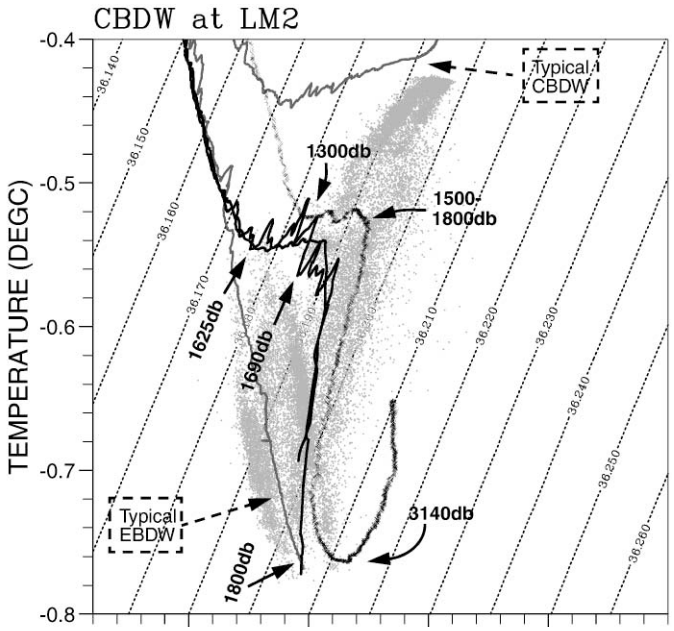

Fig. 5. In situ temperature and salinity curves from the deployment of LM2 in summer 1995 (black solid lines) showing the mixture of the deep waters from a typical EBDW profile (grey solid line to the left of the figure); and a typical CBDW profile (grey solid line to the right of the figure). Scatterplots as per Fig. 3 are included in light grey for reference. The profile from the CBDW eddy in the Amundsen Basin is also shown (line of crosses). Dotted lines are isopycnals referenced to 1731 db.

The CTD casts taken near LM3 during both the deployment and recovery cruises show that EBDW also crossed the ridge in the eastward direction. Fig. 6 suggests that an 100 to 200 m thick layer of mixed EBDW and CBDW overlies the CBDW proper. Silicate and oxygen measurements (G. Kattner, pers. comm.) suggest a mixing ratio of about 1:1. Although limited in offshore extent and observed only rarely in the LM3 time series, the EBDW inflow appears in CTD sections in both 1995 and 1996. The estimated volume transport is the same as that of the CBDW at LM2.[4] On the Canadian Basin side of the ridge, the EBDW is found only over the continental slope and not further north (e.g., it is not seen in CTD lines taken at 81°N in 1995 and 1996), suggesting that the eastward flow of EBDW either occurs through the gap at 80.4°N or just slightly to the north of LM2, where the HDNO chart shows a small channel, 3 km wide at 1600 m depth. The former route, via the larger gap, seems the most likely. We note that this gap is more than two Rossby radii wide and can thus allow simultaneous counterflows of EBDW and CBDW.

[4] Note that Jones et al. (1995), using a plume-parameterising box model of the deep Arctic Ocean, infer (larger) exchanges between the deep Arctic basins through multiple gaps in the Lomonosov Ridge. A quantitative comparison is, however, not meaningful without a revision of their model assumptions. For example, compare their boundary current transport estimate (0.5 Sv) with that of Section 3.4.

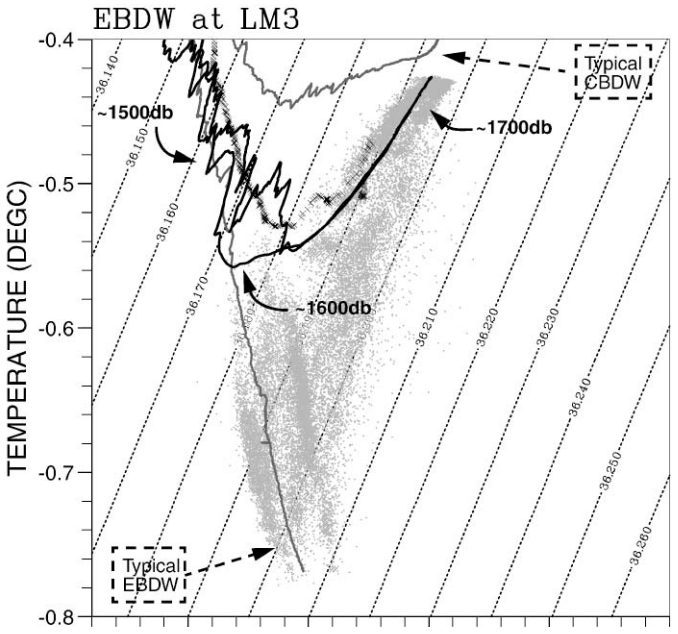

Fig. 6. In situ temperature and salinity curves from the site of LM3 in summer 1995 (black solid lines) and summer 1996 (line of crosses) showing the EBDW influence. Typical EBDW and CBDW profiles and scatter plots are as per Fig. 5. Dotted lines are isopycnals referenced to 1731 db.

3.2. Mid layer — advection of Atlantic layer core

3.2.1. Cooling of the Atlantic layer core

The warmest water in the water column is found at ~ 300 m depth, in the core of the Atlantic layer (AL), which has travelled from the Fram Strait along the slope of the Nansen Basin, being cooled by mixing with shelf waters and the overlying halocline layer (e.g., Schauer et al., 1997). North of Svalbard, the temperature of the core is $\sim 3^{\circ}$C. At LM1, the core has cooled to $\sim 2^{\circ}$C, and by LM2 and LM3, the core is still cooler, i.e., $\sim 1.5^{\circ}$C.

The most striking feature of the time series in the AL core is a sharp drop in temperature (by 1°C at LM1, by 0.7°C at LM2, by 0.5°C at LM3) and salinity (by 0.1 psu at LM1, by 0.05 psu at LM2 and LM3) which occurs at different times at the three moorings: in January 1996 at LM1, but in mid-June 1996, i.e., 140 or 150 (± 10) days later, at LM2 and LM3 (Fig. 7). We also observe a cooling at LM1 at 700 m (0.2°C), 1100 m (0.1°C) and less clearly at 1700 m. At these greater depths, the cooling event is not the dominant signal and is partly masked by other features.

The difference in the arrival times of the cooling event at each mooring suggests the signal is advected from LM1 to LM2 and LM3. Assuming the flow follows the 1700 m contour and neglecting topographic features smaller than the local first baroclinic Rossby radius (~ 7 km), the distance travelled between LM1 and LM2 or LM3 is 450 or 550 km respectively, with the paths diverging after 340 km, at the southern end of the Lomonosov Ridge. Distances are measured from the topography of HDNO (1999) and are, at best, ± 10 km. Taking the annual mean velocity at 300 m at LM1 ($5.4 \pm 0.6\,\mathrm{cm\,s^{-1}}$) as an estimate of the advection velocity for the shared part of the

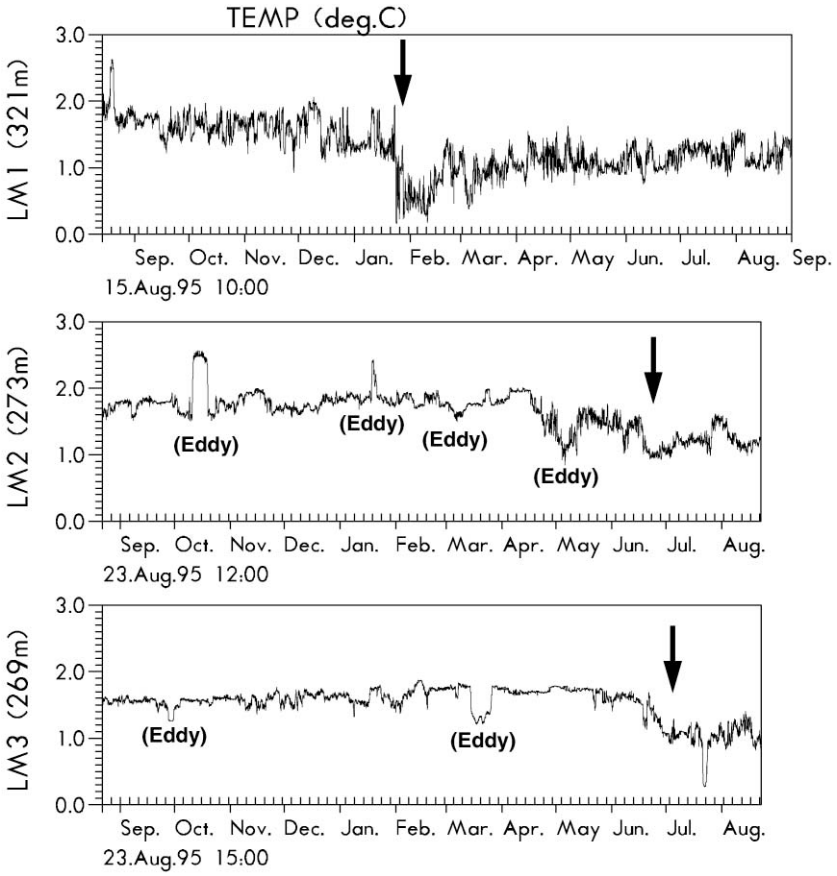

Fig. 7. Time series of in situ temperature in the Atlantic layer at the three moorings. Note the sudden cooling in late January 1996 at LM1, and in July 1996 at LM2 and LM3. Other large jumps in temperature are associated with eddies, e.g., at LM2 in October, January and May and some examples are marked on the figure.

path, and the annual mean velocity at 300 m at LM2 (1.3 ± 0.9 cm s^{-1}) and LM3 (2.7 ± 0.7 cm s^{-1}) as the relevant estimates for the remaining path to LM2 and LM3 respectively, we calculate travel times of 120 to 240 days from LM1 to LM2, and 140 to 210 days from LM1 to LM3, estimates which bracket the time delays observed between the arrival of the cooling at the different moorings. Further, a CTD section across the Lomonosov Ridge at 82.5°N taken in August 1996 found only the warmer version of the AL. This section is 150 km north of LM2, which for a mean velocity of 1.3 ± 0.9 cm s^{-1} requires a travel time of at least 2.5 months. Thus, a signal first observed in June at LM2 would not be seen at 82.5°N until at least September.

What is the cause of this cooling and freshening? On T–S diagrams (Fig. 8), the modification of the AL between 1995 and 1996, along with small, almost isopycnal steps in temperature and salinity, suggest isopycnal mixing with water in a temperature and salinity range typical of the Barents Sea shelf (Swift et al., 1983; Loeng et al., 1993).

Using CTD data from 1993, Schauer et al. (1997) show a similar isopycnal change and infer that the warm core of the Atlantic water that has passed through the Fram Strait (Fram Strait Branch

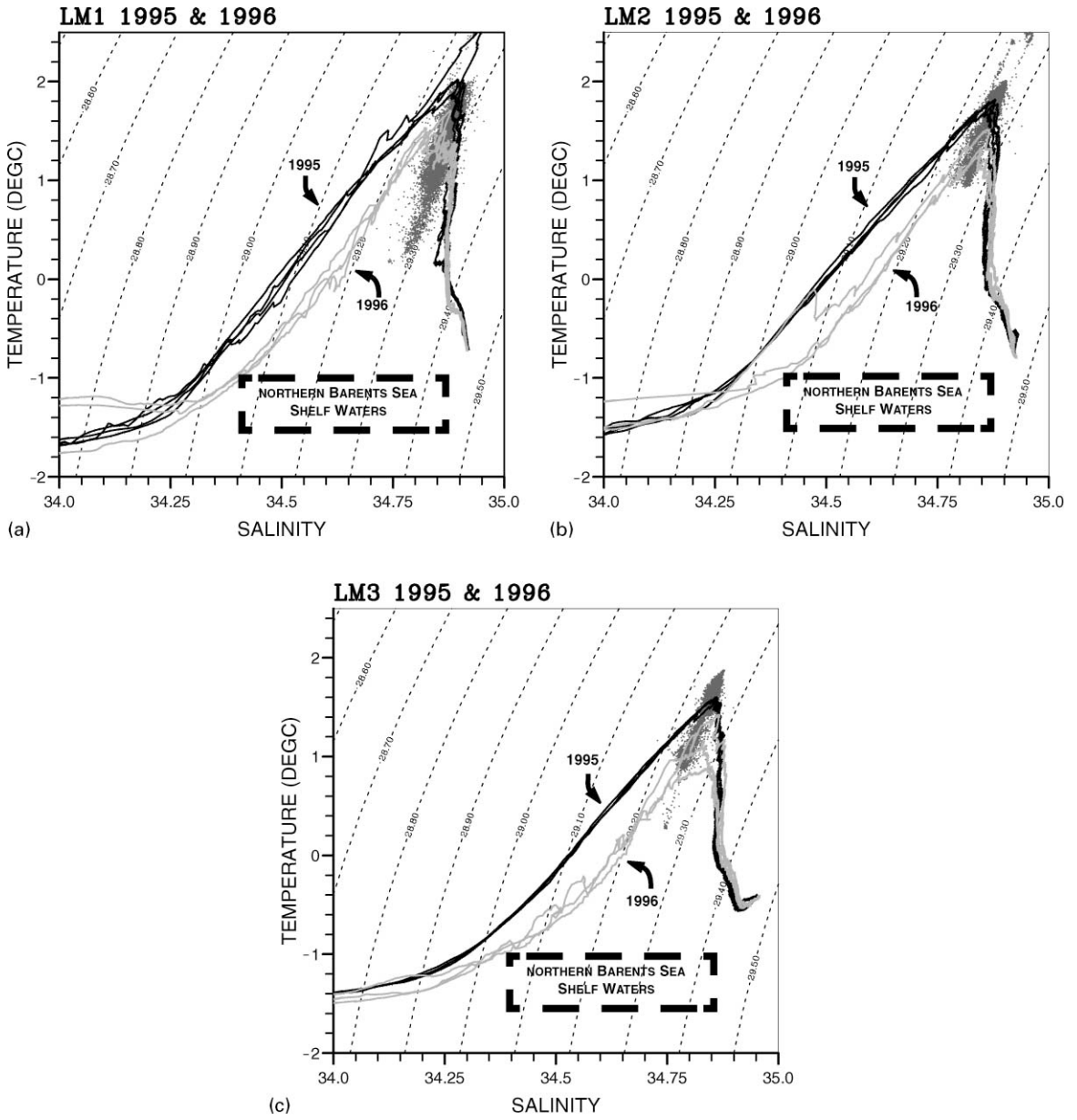

Fig. 8. In situ temperature and salinity curves at (a) LM1, (b) LM2 and (c) LM3, showing, for each mooring, the SBE 1-hourly data from $\sim$ 300 m over the year-long deployment (grey dots), CTD stations taken near the mooring site at the deployment in summer 1995 (black solid lines) and at the recovery in summer 1996 (grey solid lines). Dotted lines are isopycnals referenced to 290 db, the average pressure of the three instruments. The area marked by the dotted rectangle indicates the approximate T–S properties of the cold waters found on the northern Barents Sea shelf.

Water, FSBW) mixes over depth ranges of 200 to 1000 m with the modified waters of Atlantic origin that have passed through the Barents Sea (Barents Sea Branch Water, BSBW) in roughly equal parts.

The cooling and freshening we observe is most likely due to a change in properties or volume of an end member of this mixing process. For example, it could result from a cooling and freshening of the FSBW or a decrease in the volume of FSBW relative to BSBW. We can discount the former possibility, since time series of temperature from Sørkapp, Spitsbergen, show no decrease in temperature for the time in question, (Blindheim et al., 2000). We lack the data to test the latter possibility directly, although it seems unlikely since both CTD and mooring evidence point to an increase in the amount of water entering the Arctic via Fram Strait in the 1990s (Rudels et al., 2000a; Woodgate et al., 1998). Therefore, we instead hypothesise the cooling and freshening is due to a change in the quantity and/or properties of the waters that exit the Barents Sea to intrude and mix into the AL.

To test the viability of this hypothesis, we estimate the extra volume of cold, fresh shelf waters that would be required and the T–S transformations necessary to form this extra volume of cold, fresh water from the warm, salty Norwegian Sea inflow to the Barents Sea. From Fig. 8, the coldest water observed in the AL (the extreme points of the scatterplot) suggest, at most, a 1 : 1 mixing of cold, fresh shelf waters with the AL core. For a resulting 100 km wide core, 300 m deep and moving at $5\,\mathrm{cm\,s^{-1}}$ (~ 1.5 Sv), this would require an additional cold, fresh outflow from the Barents Sea of 0.8 Sv. This is within the observed variability of the Barents Sea net outflow, which has been estimated by Loeng et al. (1993) to vary seasonally between 1 and 3 Sv. Assuming the mean velocity of the AL at LM1 is representative of the flow from St. Anna Trough to LM1, and estimating the path length as between 1100 and 1400 km, the additional cold water must have emerged from the St. Anna Trough 8 to 11 months earlier (i.e., between February and May 1995), and from the Barents Sea ~ 4 months prior to that (i.e., between October 1994 and January 1995). Thus, to give the cooling and freshening observed, the output from the Barents Sea would have had to be colder and fresher in winter 1994–1995 than in winter 1993–1994. Changes in precipitation minus evaporation (P–E) in the Barents Sea for this time period estimated from satellite data (D. Groves, pers. comm.) are too small to account for the freshening. In fact, the amount of extra freshwater required is approximately equal to the total annual value of P–E (see also Gorshkov, 1983). Data from the International Arctic Buoy Programme (IABP) (I. Rigor & M. Ortmeyer, pers. comm.), however, suggest that between summer 1994 and summer 1995 the inflow of ice to the Barents Sea was almost twice that of the previous year. Melting this extra ice could cool and freshen the waters in the Barents Sea sufficiently to match the observations (for details, see Appendix B). While these are by necessity crude estimates, they show that a change in the flux of ice into the Barents Sea of the magnitude observed could easily give rise to the observed changes in the AL, and, as will be discussed in Section 3.3 below, could also be the cause of further changes in T–S properties of other waters carried by the boundary current.

3.2.2. Pathway of the Atlantic layer core

Except for the flow along the continental slope, the pathways of the AL into the Canadian Basin have not been well defined by past surveys. In particular, the flow along the Canadian Basin side of the ridge is very poorly known. The CTD data presented here (combined with older measurements) suggest the AL flows over the Lomonosov Ridge, not only at the most southern end of the ridge,

but also further north. In particular, CTD sections across the Lomonosov Ridge at 81°N in 1995, and at 81°N, 82.5°N and 86.5°N in 1996, show water warmer than 1.4°C on the Canadian Basin side of the ridge. Water this warm was not observed further north, however, e.g., at 88°N and 88.8°N during the 1994 Arctic Ocean Section (Swift et al., 1997), at ~88°N during the 1991 *Oden* cruise (Anderson et al., 1994), nor in the 1995 SCICEX data (Boyd et al., 1997), although the station spacing of the latter might have missed the core. The implication is that warm AL water has passed over the ridge south of 88°N and is moving southward on the Canadian Basin side, forming part of an elongated anticyclonic gyre over the ridge. This ridge overflow may be a result of topographic steering. For example, the topographic map of HDNO (1999) shows a channel of maximum depth ~1300 m through the ridge at ~86.6°N, and it is possible there are other uncharted gaps as well, although the absence of warm AL water north of 86.5°N suggests that the warm water does not cross the ridge in significant quantities north of that latitude. This implies that the large gap at ~88°N shown in both the HDNO (1999) and the NRL (Perry and Fleming, 1986) maps does not reflect the true topography, a conclusion supported by the SCICEX 1999 topographic data (Coakley et al., 1999), which shows the gap to be both shallower and blocked by shallower topography on the Canadian Basin side.

3.3. Top layer — changes in the halocline

The shallowest instruments on the moorings were placed at ~100 m, nominally at the base of the cold halocline. In this layer, which lies below the ~50 m thick surface mixed layer, the temperature is almost constant, whilst the salinity increases rapidly with depth. On a T–S plot, this lower halocline water (LHW) is found as a sharp bend at salinities of between 34.2 and 34.4 psu and temperatures of −1°C or colder. Noting that this water cannot be formed by a direct mixture of the waters above and below, Aagaard et al. (1981) suggest an advective source for this water, viz., that cold, salty waters from the shelves interleave in the water column above the warmer Atlantic layer and below the cold, but fresher mixed layer. Rudels et al. (1996) propose instead that the halocline consists of water originating from winter convection north of the Barents Sea, which is subsequently covered by low salinity shelf water north of the Laptev Sea, i.e., that the cold mixed layer in winter extends to the base of the halocline, and that low salinity waters are advected in at the surface to form the cold halocline. Steele and Boyd (1998) suggest a combination of these mechanisms, remarking that the distinction between the two mechanisms is the origin of the lower halocline water, i.e., whether it is advective (Aagaard et al., 1981) or convective (Rudels et al., 1996).

This issue may, in fact, be resolved by the different thermal signatures these processes leave in the water column. If the LHW is formed by convection, then the water at the top of the thermocline will be near the freezing point, since it is the salt rejection on freezing that drives the convection. In contrast, an advective source for this LHW does not necessarily result in a halocline at the freezing point. The distinction is well illustrated by a line of CTD casts (Fig. 9) taken in 1993 near section C (for location, see Fig. 1). The deeper casts (in water depths greater than 2500 m) show a comparatively fresh halocline with temperatures near the freezing point. This may have a convective origin. At stations nearer to the shelf (those shallower than 1200 m), the cold halocline layer is warmer and saltier, and is most probably of shelf origin. Intermediate depth stations show some features of both haloclines. Thus, we conclude that shelf processes form the halocline in the

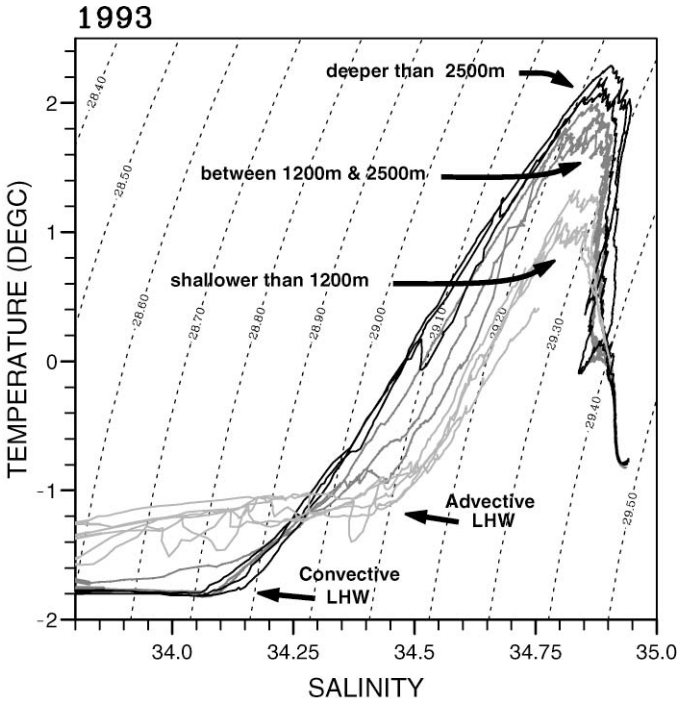

Fig. 9. In situ temperature and salinity curves for September 1993 CTD section running from 79.2°N to 77.2°N along ~ 118°E, (see Fig. 1). Light grey profiles are the six stations nearest to the continental shelf, in water depths less than 1200 m, showing the warmer upper layers and the deeper cold halocline with shelf origins. Black curves are the deepest three stations, in water depths greater than 2500 m, with upper layers near the freezing point, suggesting a convective origin for the halocline water. Dark grey profiles mark the three stations in the intermediate depths which show evidence of both haloclines. Dotted lines are isopycnals referenced to 290 db.

boundary current, whilst in the deeper water, convection can play a role, although we cannot ascertain if the convection has occurred locally.

The presence of the cold halocline layer in our sections in 1993 (Fig. 9) and 1995 and 1996 (Fig. 8, Appendix C and below) is noteworthy since Steele and Boyd (1998) report the retreat of the cold halocline from the central Eurasian Basin in the 1990s, relating this to a change in the wind patterns, which caused the shelf waters to be advected further eastward along the shelf and continental shelf break rather than into the central Arctic.

While our moored instruments are too deep to measure the evolution of the cold halocline itself, trends in the records, combined with CTD data, show long-term (i.e., longer than seasonal) changes in the structure of the upper ocean. The shallowest (~ 100 m) temperature and salinity time series on all three moorings show an almost linear increase in temperature, salinity and density over the year. This is most marked at LM2 and LM3 (changes in temperature and salinity of 0.18°C and 0.19 psu, and 0.15°C and 0.25 psu, respectively), although a similar trend is found at LM1 also (change in temperature and salinity of 0.05°C and 0.1 psu). The effect is to raise the cold halocline layer. The changes are small: the temperature change could result from an additional heat flux of about 2 $W m^{-2}$ over the year, whilst the salinity change is equivalent to formation of 0.5–1.0 m of

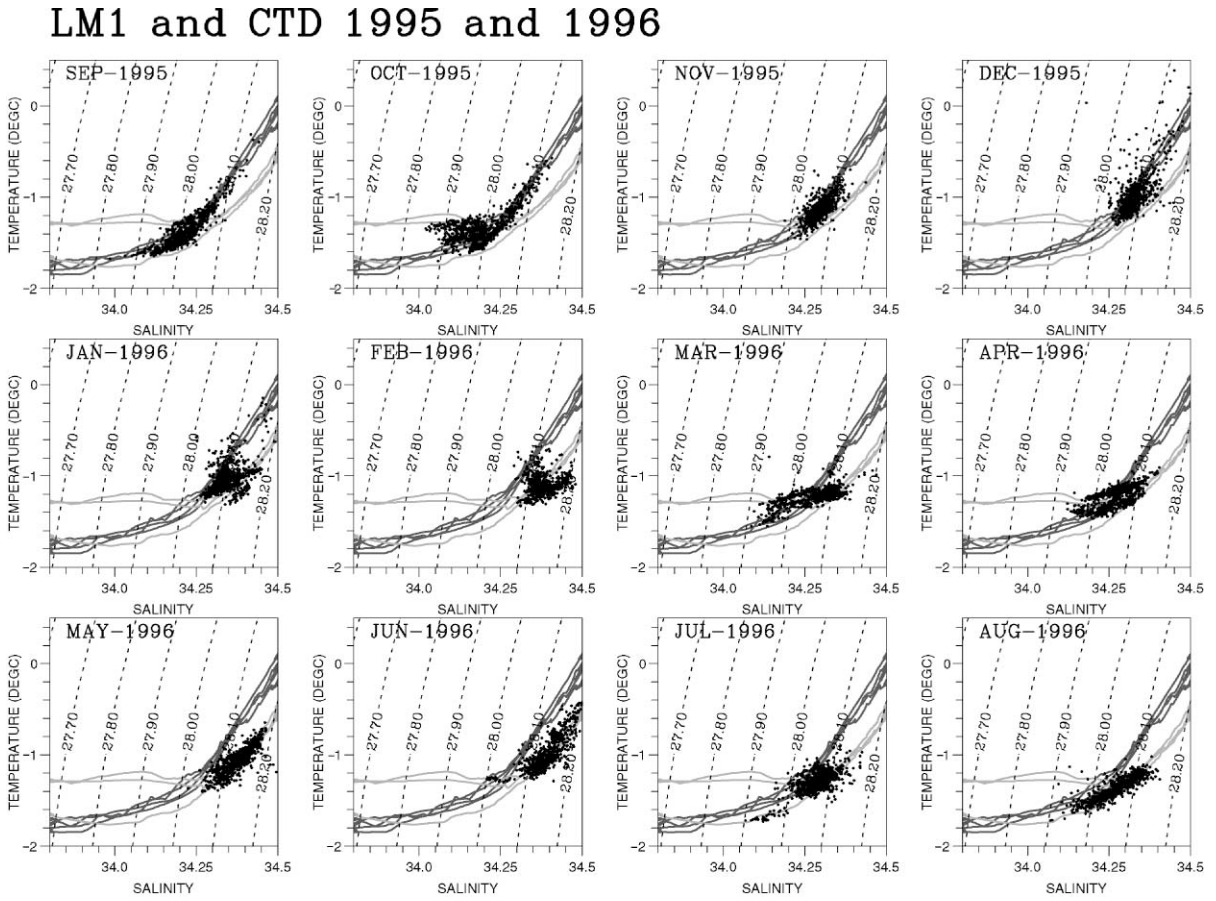

Fig. 10. In situ temperature and salinity curves at LM1 showing the SBE 1-hourly data from ~ 100 m for each month over the year-long deployment (black dots), CTD stations taken near the mooring site at the deployment in summer 1995 (dark grey solid lines) and at the recovery in summer 1996 (light grey solid lines). Dotted lines are isopycnals referenced to 100 db.

ice or the removal of 0.3–0.6 m of freshwater. The gradual nature of the change and its presence at all three sites is, however, remarkable and suggests a non-local process.

The conservation equations for heat and salt, when scaled, suggest that the vertical and horizontal advection and diffusion terms may all be first order. We can discount vertical diffusion as the dominant process for the warming and salinisation, however, since the negative value of $\partial^2 S/\partial z^2$ at halocline depths would drive a decrease rather than an increase in salinity.[5] Combining the SBE data with the CTD casts (Fig. 10) suggests instead that vertical advection dominates, i.e., that the changes are due to a raising of the isopycnal surfaces, since the time series data lie predominantly on the T–S curve of the deployment or recovery CTDs. Due to the sharp vertical

[5] This assumes the diffusion coefficient (κ) is constant. In reality, the eddy diffusion depends on the density gradient, being less in the upper layers where the density gradient is high. Thus, a suitable increase in κ could overcome a local decrease in $\partial S/\partial z$. Numerical trials suggest, however, that to achieve this, the form of κ would have to be an extreme function of the density gradient.

gradients near 100 m, raising an isopycnal by only 30 m would give the observed changes in temperature and salinity. Over one year, this is equivalent to a vertical velocity of 1×10^{-7} m s^{-1}, comparable in magnitude to the annual average Ekman pumping velocity (curl $\tau/(\rho_o f)$) estimated from 6-hourly NCAR data, where τ is the wind stress estimated by a simple drag law, ρ_o is water density and f is the Coriolis parameter. The calculated Ekman velocity, however, does not exhibit the quasi-steady nature observed in the temperature and salinity data and, moreover, is downward rather than upward. We suggest instead that the isopycnals are raised by the intrusion of another water mass below the depth of the upper instrument. If we consider a boundary current 100 km wide, moving at 5 cm s^{-1}, the transport required to inflate a 30 m thick layer is ~ 0.2 Sv, which is only 20% of the hypothesised extra inflow of Section 3.2. The associated vertical motion would not result in comparable T–S changes at the deeper instruments, since the vertical gradients of temperature and salinity are less there. Furthermore, the gradual change at ~ 100 m can be reconciled with the sudden change observed at ~ 300 m if the entry depth of the shelf intrusion changes. For example, if initially the cold shelf water enters at some depth below 100 m but above 300 m, one would observe the raising of the isopycnals at 100 m but little or no change at 300 m. If the entry depth of the cold water increased to beyond 300 m, then the sudden change would be observed at 300 m, while the slow trend would continue at 100 m.

Therefore both the cooling and freshening at 300 m and the warming and salinisation at 100 m can be driven by increased cold outflow from the Barents Sea in winter 1994–1995, which intruded into or below the halocline and was advected along the continental slope. This reconstruction is further supported by a progression of CTD sections (Figs. 11a–e) taken across the continental slope in August 1995 (locations shown in Fig. 1), which show the same changes in T–S properties between locations progressively further westward as are seen at the mooring sites in increasing time. In 1995 at LM1 and at the easternmost CTD section (D), the warmer, deeper halocline (i.e., with temperatures above zero at a salinity of 34.5 psu) is present. This is the warm phase, seen in the early part of the moored time series. At the westernmost CTD sections (A and B), the more prominent, shallower halocline is evident as a sharp bend in the T–S curve near the salinity 34.5 psu and an increased salinity in the immediately underlying waters. This is the cold phase, seen later in the moored time series. (Note that the warmer outliers of Fig. 11a represent stations in the deeper water away from the slope, where the shelf influence is less.)

From the presence of the cold signal at sections A and B, and its absence at section D, we can bracket the speed of propagation of this colder water to between 6 and 1 cm s^{-1}, since, from the mooring data, we know it arrived at LM1 in January 1996. If the front had only just reached section C at the time of the CTD section, the speed is 4 cm s^{-1}. These numbers agree well with the mean velocity measured at LM1 (~ 5 cm s^{-1}), but are much greater than the apparent advection speed of about 1 cm s^{-1} calculated by Frank et al. (1998). The latter, however, is deduced from the CFC age and does not take into account the mixing of the boundary current waters with older water from the interior. This mixing increases the CFC age; thus, ignoring it results in velocity estimates which are too low.

A secondary issue is that, as the shelf intrusion is advected towards LM1, the shape of the T–S curve changes. For example, comparing section A in 1995 with the 1996 CTD stations taken near

[6] Note that this is close to being the same water column as it takes almost a year to advect water from the St. Anna Trough to LM1.

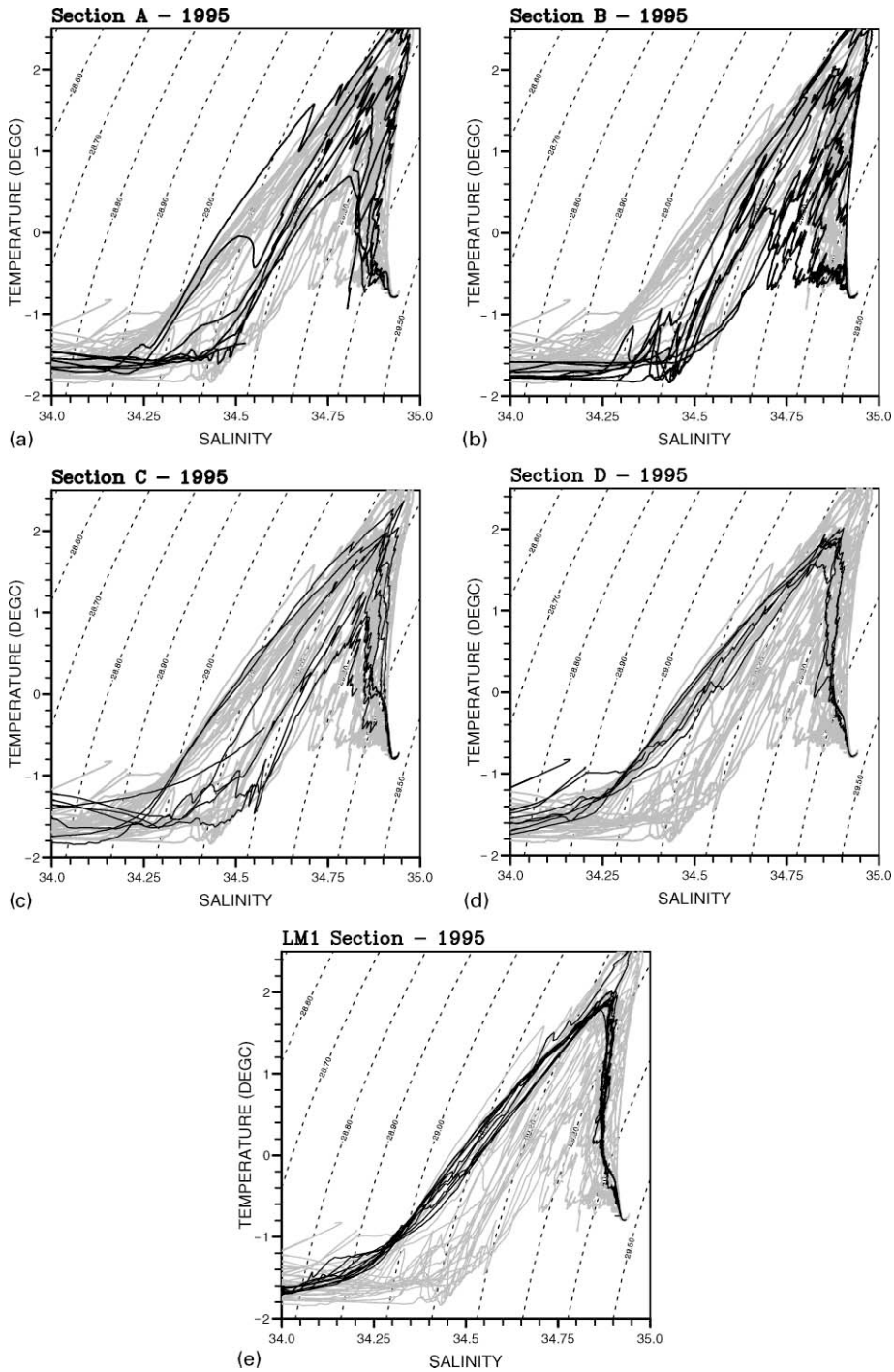

Fig. 11. In situ temperature and salinity curves for August 1995 CTD sections along the continental slope. Black lines mark the casts at the stations in (a) section A, (b) section B, (c) section C, (d) section D and (e) the section at LM1, see Fig. 1 for locations. The grey lines are the conglomeration of all the casts from these five figures for reference. Dotted lines are isopycnals referenced to 290 db.

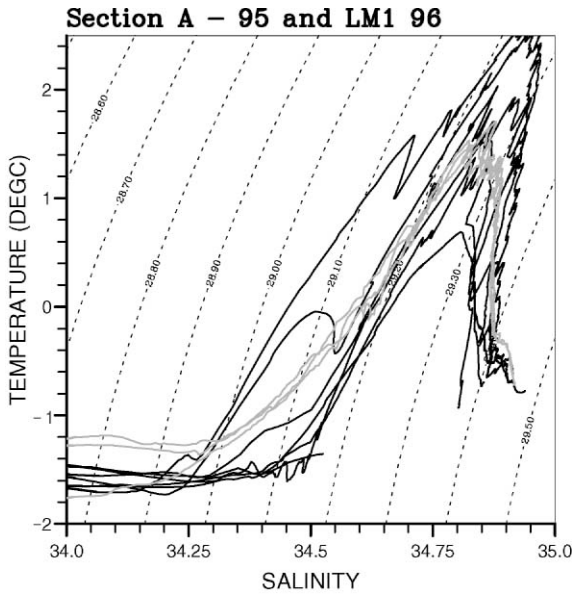

Fig. 12. In situ temperature and salinity curves for CTDs at section A in 1995 (black lines) (cf. Fig. 11a) and LM1 in 1996 (grey lines) showing how the sharpness of the T–S curve has been eroded during the transit from section A to LM1. Dotted lines are isopycnals referenced to 290 db.

LM1 (Fig. 12),[6] we see that the sharp T–S corner near salinity 34.5 psu has been eroded as the water moves downstream. This may be the result of mixing with adjacent waters, e.g., at LM1, with waters from the interior (cf., the outliers in Fig. 12) or at LM2, with waters from the other side of the ridge (cf., one of the 1996 stations in Fig. 8b, which shows the older, warmer water on the Canadian Basin side of the ridge). Alternatively, the T–S curve may have been smoothed by vertical diffusion. A simple diffusion model ($\partial(T,S)/\partial t = \kappa\partial^2(T,S)/\partial z^2$) gives the observed change in sign and magnitude over a few months using diffusion coefficients (κ) of order $4\times10^{-5}\,\mathrm{m^2\,s^{-1}}$, well within the range of coefficients suggested by Dewey et al. (1999).

3.3.1. Discussion

We conclude that the T–S changes at the three mooring sites are most likely caused by changes in the outflow from the Barents Sea. This reconstruction indicates that comparatively small changes in the outflow from the Barents Sea can have far reaching effects on the T–S structure of the Arctic Ocean.

There are three main implications. The first is the observed strengthening of the cold halocline, which contrasts with the retreat of the cold halocline from the interior Eurasian Basin reported by Steele and Boyd (1998). The second implication is the indication that in this region the cold halocline layer is maintained by an advective shelf source, as opposed to a local convective source (compare Aagaard et al., 1981; Rudels et al., 1996; Steele and Boyd, 1998). The third implication is a possible feedback mechanism related to ice formation in the Arctic Ocean. In this feedback, ice exported from the Arctic Ocean cools and freshens waters in the Barents Sea, and these waters, on

exiting into the Arctic Ocean, strengthen the cold halocline in the eastern Arctic. This strengthening of the cold halocline inhibits heat flux from the Atlantic layer to the surface and hence promotes ice growth. Thus, the export of ice from the Arctic Ocean can indirectly, and with some time-lag, promote the growth of ice elsewhere in the basin.

3.4. Equivalent barotropic flow and transports

3.4.1. Vertical structure

The equivalent barotropic nature of the flow noted in Section 2.2 can be formalised by an EOF analysis of the filtered data (Fig. 13 and Table 2). (The filtered data are used since we are interested in the vertical structure of the current, not the vertical structure of the tides.) At all three moorings, the first EOF, which explains over 70% and usually almost 80% of the variance of the filtered data, has a very similar equivalent barotropic structure in the vertical. By decomposing the EOFs onto the vertical normal modes of the system (e.g., Gill, 1982),[7] we find about half of the first EOF can be attributed to the barotropic mode (which is essentially depth-independent[8]), the remaining half consisting of comparable weightings of the first three baroclinic modes. Only four mode weightings can be determined, since there are only four points in the vertical.

Geostrophic velocity profiles below 100 m, calculated from the CTD profiles, generally show a vertical structure similar to the EOFs. This suggests that linear interpolation between the four instrument depths gives a reasonable approximation to the actual flow[9]. Above 100 m, the geostrophic velocity shear often shows a reversal in sign. A coherent boundary current is not evident from the geostrophic shear profiles, however. This is probably due to a combination of circumstances, both observational (e.g., that the CTD stations are widely separated in space and time; that the CTD sections are often not aligned perpendicular to the flow, and that there are eddy and meander features) and dynamical (e.g., that the barotropic part of the flow is as large as the baroclinic and that the barotropic velocity presumably varies across the current). Therefore, geostrophic transport estimates relying on an assumed level of motion will be significantly in error.

3.4.2. Estimate of the transport

The similarity of the vertical structure of the current at all three mooring sites, obtained both from RCM measurements and from the baroclinic shear estimated from sections taken across the current, suggests that this vertical structure is characteristic of the boundary current. This gives a basis for estimating the transport.

We assume that the depth-averaged velocity at each mooring is representative of the barotropic flow at all points across the boundary current in that cross-section. In reality, the barotropic velocity will presumably vary across the current, vanishing at the edges of the current. As we have no information on how the barotropic velocity varies across the current, we assume it is constant

[7] The normal modes are obtained from CTD profiles near the mooring sites and yield barotropic/baroclinic wavespeeds of 130, 1, 0.6 and 0.3 $m\,s^{-1}$ corresponding to Rossby radii of $\sim$ 900, 7, 3 and 1.5 km, respectively.

[8] Thus, numerically, the barotropic flow and the depth-averaged flow are equivalent.

[9] Note that the CTD data are only from the summer. There is, however, no indication from the current meter data of a significant change in vertical structure in other seasons.

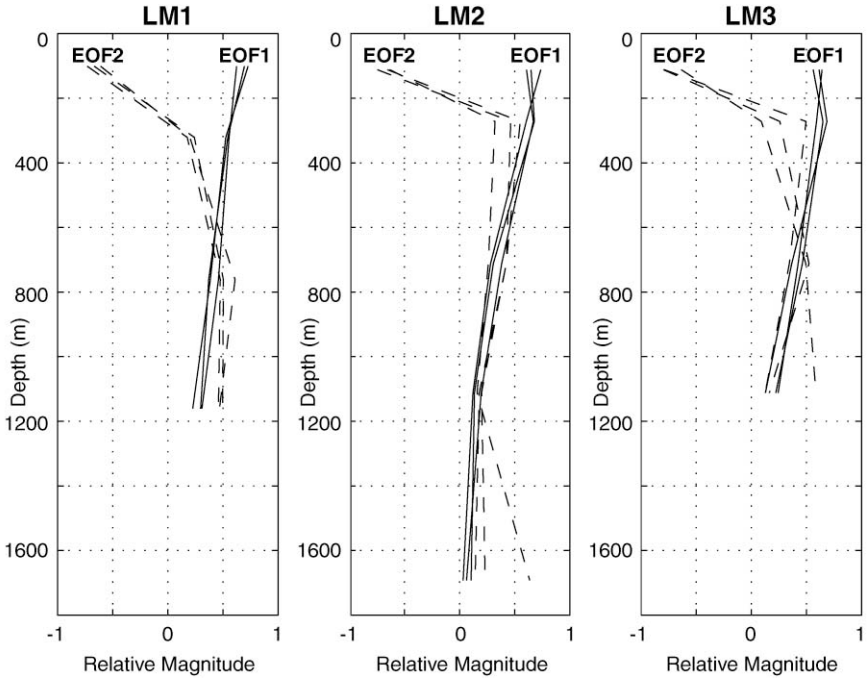

Fig. 13. First (solid lines) and second (dashed lines) EOFs with depth for filtered speed and eastward and northward components of filtered velocity at LM1 (left), LM2 (middle) and LM3 (right).

Table 2
EOF analysis of filtered data[a]

% Variance explained by	LM1			LM2			LM2			LM3		
	U	V	Speed	U	V	Speed	U	V	Speed	U	V	Speed
EOF1	81	77	71	87	83	80	79	78	76	80	79	75
EOF2	13	16	20	10	12	16	11	11	15	11	14	14
EOF3	4	5	6	2	4	3	7	8	5	7	5	8
EOF4	2	2	3	1	1	1	2	3	3	2	2	3
EOF5	N/A	N/A	N/A	N/A	N/A	N/A	1	1	1	N/A	N/A	N/A

[a]For LM2, the analysis is done twice, once (left) using the top four current meters for better comparison with LM1 and LM3, and once (right) using all five current meters. N/A = not applicable.

within the current and zero outside the current. In the annual mean, the depth-averaged velocities at LM1, LM2 and LM3 are 4.4, 1.2 and 1.9 $cm\,s^{-1}$, respectively (all $\pm 1\,cm\,s^{-1}$). These are weighted averages of the currents at the top four current meters. At LM2, there is a fifth current meter ~ 20 m above the bottom, but including this record in the average only changes the mean velocity to 1.3 $cm\,s^{-1}$, well within the errors of this calculation. We consider the warm Atlantic

layer as a tracer for the boundary current and estimate the horizontal width of the current as the across-slope extent of the warm core (defined as water within 0.2°C of the maximum temperature found on the CTD section). This width cannot be determined directly from the CTD sections since they do not run perpendicular to the coast. Instead, from the CTD sections, we first estimate the water depths over which the warm core is found (typically $\sim$ 500 to 3000 m). Then we determine the lateral separation of these water depths along an imaginary section perpendicular to the topography (and the mean flow) at each mooring location, using the HDNO (1999) chart. At LM1, the water depth range is $\sim$ 500 to 3000 m; at LM2, the range is 3000 m to the top of the ridge at 1500 m; at LM3, the range is 500 to 2500 m. (Note that these depth ranges are consistent with the boundary current being split by the topography of the ridge, i.e., the part of the current over the deeper water is directed northward by the ridge, whilst the part of the current over the shallower water continues on eastward into the Canadian Basin.) This procedure leads to estimates of the current width as between 50 and 84 km at LM1, 100 and 130 km at LM2 and 90 and 100 km at LM3. Combined with the water depth information and the depth-averaged velocities, these widths give transport estimates of 5 ± 1 Sv at LM1, 3 ± 1 Sv at LM2 and 3 ± 1 Sv at LM3. These numbers suggest the current is split into comparable parts by the Lomonosov Ridge intersecting the continental slope.

Fig. 14 collates these transports with estimates and pathways discussed earlier in the text. Other observational estimates of the boundary current transport are hard to find. At best, we can consider the sum of the input from the Barents Sea (1 to 3 Sv, Loeng et al., 1993) and the input from the Fram Strait. Estimates of the latter vary significantly, e.g., 5.6 Sv (Hanzlick, 1983), 3 ± 1 Sv (Jónsson, 1989) and 7 ± 2 Sv (Woodgate et al., 1998). The last estimate may reflect a recent substantial increase in the Atlantic input to the Arctic via the Fram Strait (Woodgate et al., 1998; Rudels et al., 2000a). For our purposes, however, given the errors involved, the boundary current transports estimated above are not inconsistent with the sum of the two separate contributing branches.

A comparison of these results with the increasing number of high-resolution (order 10 km) numerical models of the Arctic circulation is qualitatively illuminating. Most primitive equation models, e.g., OCCAM (A. Coward, pers. comm.) and the PGS Monterey model (W. Maslowski, pers. comm.), show the barotropic slope current to continue mainly into the Makarov Basin rather than being split by the Lomonosov Ridge. The exception is the model of Nazarenko et al. (1998), which achieves a splitting of the current (and strong boundary currents around the periphery of the basins) by including a subgridscale parameterization of the interaction of eddies and topography (the 'Neptune' effect, Holloway, 1987). The success of the latter approach suggests that mesoscale features (discussed in Section 3.5 below) may be important to understanding the dynamics of the boundary current.

3.5. Mesoscale features

The strongest currents at all three mooring sites occur in isolated events which last about two weeks at LM2 and LM3 (less at LM1), often extend through the water column and are usually accompanied by a temperature and salinity anomaly. Turning of the current with time indicates the passing of an eddy or meander. Since the events are so dominant in the velocity, temperature and salinity data (e.g., Figs. 2 and 7), an overview will be given here, although a full analysis is beyond the scope of this paper. Fig. 15 catalogues the events, using the selection criteria of a speed anomaly exceeding $5\,\mathrm{cm\,s^{-1}}$ and a turning in direction of at least 90°.

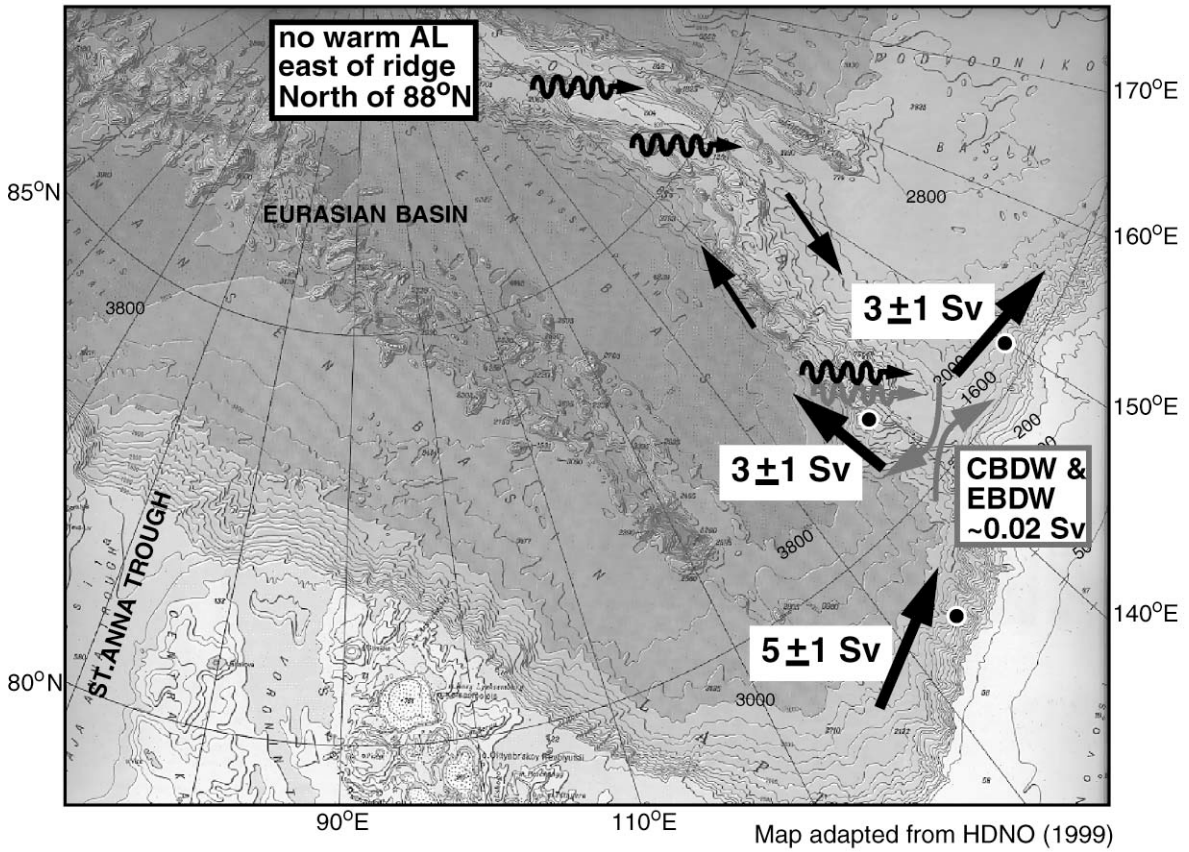

Fig. 14. Schematic map of the transports and pathways discussed in the text. Straight black arrows indicate the direction of the depth-averaged flow. At the mooring sites, the arrows (thick black) are labelled with the total transports. Grey arrows indicate the exchanges of the deep waters. Grey squiggly arrows indicate a possible alternative path for the deep waters across the Lomonosov Ridge. Black squiggly arrows indicate possible pathways of the Atlantic layer.

The velocities peak at $40\,\mathrm{cm\,s^{-1}}$, being usually greatest in the upper layers ($\sim 100\,\mathrm{m}$ and $300\,\mathrm{m}$) and generally weaker ($\sim 10\,\mathrm{cm\,s^{-1}}$) at the lower meters. The geostrophic velocity shear calculated from the density field of the Amundsen Basin eddy of Section 3.1 shows a velocity anomaly at the depth of the eddy of only $4\,\mathrm{cm\,s^{-1}}$, indicating that either the station spacing underestimates the sharpness of the front, or the motion has a significant ageostrophic or barotropic component (cf., Manley and Hunkins, 1985). For the events observed at the moorings, the length scale of the features (quasi the diameter) can be estimated from the duration of the event, viz., (2 weeks $\times 1.5\,\mathrm{cm\,s^{-1}} =$) 18 km, which is consistent with the eddy having a radius similar to the first baroclinic Rossby radius, 7 km. (The second baroclinic Rossby radius is $\sim 3\,\mathrm{km}$.) The rotation sense, determined as by Foldvik et al. (1988), is generally anticyclonic, a predominance found both in other observations (Manley and Hunkins, 1985) and in modelling studies (e.g., Jungclaus, 1999). At LM2 and LM3, about five clear eddy events occur during the year-long deployment. At LM1,

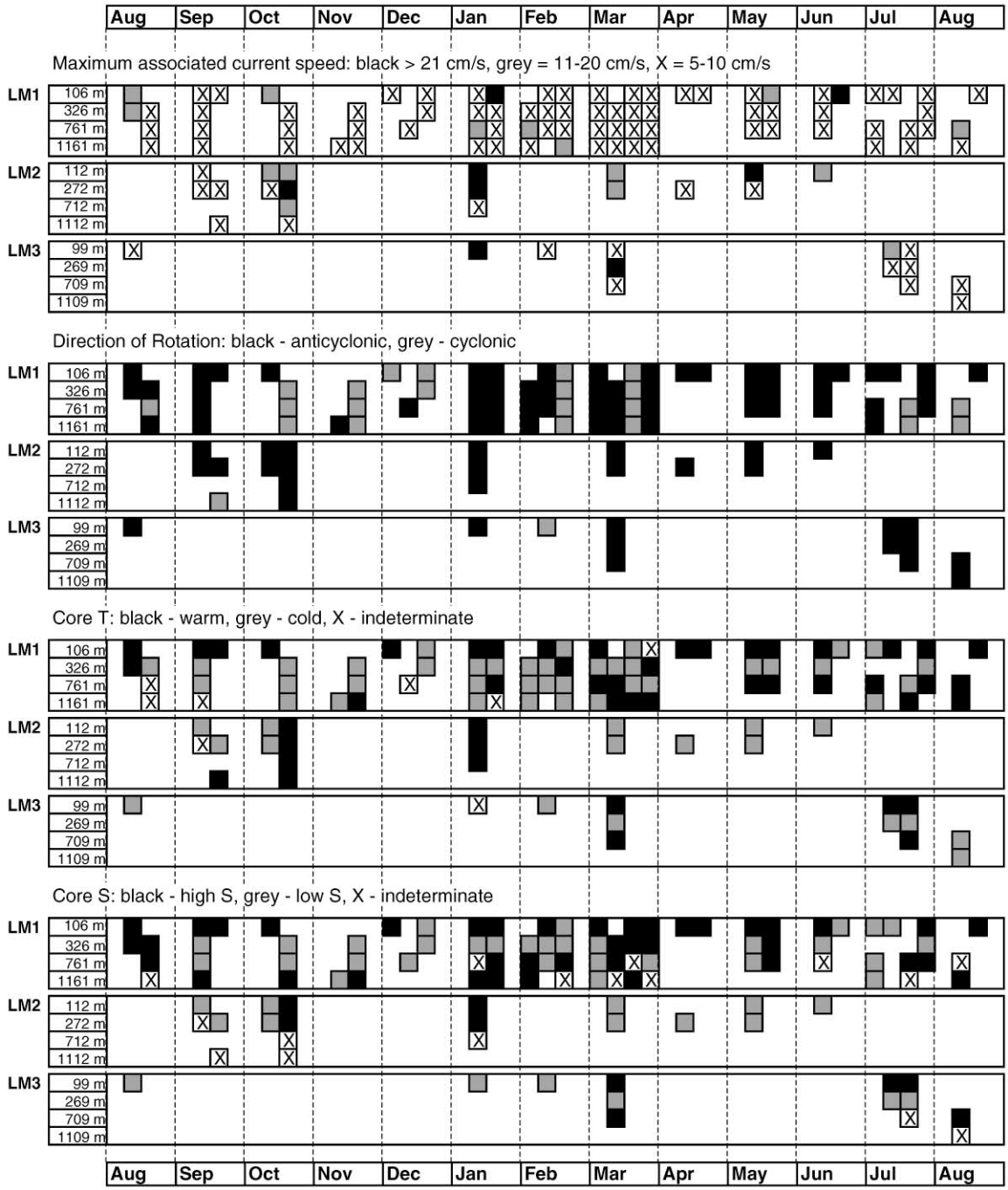

Fig. 15. Summary of eddy characteristics.

although there are about the same number of strong events, they are not as prominent in the records, due to an almost continuous series of weaker events.

Predominantly, two different types of eddies are observed. Examples of the first are confined to the surface layer (e.g., at LM3 in January, at LM2 in May and June), invariably show a cold, low salinity T–S core anomaly and, with one exception (at LM3 in February), are anticyclonic. The shallowness of the eddies and the properties of the core, viz., frequently near the freezing point and often comparatively homogeneous, suggest the formation mechanism modelled by Chapman (1999), which creates cold core eddies in the mixed layer and upper pycnocline via instabilities of the front between the dense waters formed under a wind-forced coastal polynya and the surrounding shelf waters. (Note that although the water in the polynya is more saline than the surrounding shelf waters, the polynya water is fresher than waters of the same density over the slope.)

The second type of eddy extends over 1000 m or more of the water column (e.g., at LM2 in October, which extends down to at least 20 m above the bottom). Most examples show a warm, salty anomaly and a decrease in strength with depth, although the strongest flows may be at ~ 300 m rather than at ~ 100 m. These eddies are, again, predominantly anticyclonic. The large depth range suggests they are formed from instabilities of a front with a similar vertical extent. The most obvious such front is that formed between the FSBW and the BSBW in or near the St. Anna Trough. This front will be sharpest (and hence most unstable) in its formation region. Downstream, horizontal mixing between the FSBW and the BSBW erode the front, leaving no clear horizontal distinction between the two branches. Although we lack sufficient data to do a full instability analysis of the front, using CTD and LADCP data from near the St. Anna Trough collected on the Polarstern 1996 cruise to estimate the instability conditions suggested by Killworth (1980) and Mysak et al. (1981), we conclude that the region may be prone to instability. If this is indeed the formation area, the eddies will be ~ 16 months old when they reach the moorings. This is not unreasonable since Manley and Hunkins (1985) suggest lifetimes in excess of 13.5 months for eddies in the Beaufort Sea.

At LM2, the only mooring with a RCM 20 m above the bottom, there is some evidence of deep eddies or meanders which do not have a signal in the water column above (e.g., in March and April). Although there is no consistent T–S anomaly associated with these increases in current speed, the features may relate to the deep water exchanges and the Amundsen Basin eddy discussed in Section 3.1.

Previous discussions of Arctic eddies (Newton et al., 1974; Manley and Hunkins, 1985, and D'Asaro, 1988) consider eddies in the Canadian Basin. The measurements we present are the first catalogue of surface and deep eddies from the continental slope of the Eurasian Basin. Whilst the eddies are the largest signals in the temperature, salinity and velocity records, their direct impact on the mean circulation is probably small. In transport terms, they represent a volume flux of, at most, ~ 0.1 Sv, (considering five full depth eddies over one year), a small fraction of the total along-slope current. They may, however, represent a significant across-slope advection. The horizontal eddy heat flux per unit area averaged over the record at each current meter, calculated as $\rho_o c_p \overline{u'T'}$ (where c_p is the specific heat capacity of water and u', T' are the deviations of the across-slope velocity and the temperature from the record-length mean), is of order 1 to 10 kW m^{-2}. Whilst this is sufficient to warm an 100 km wide core of water between 0.03 and 0.3°C, the uncertainty in this flux is greater than the flux itself, and the calculation can only be taken as a rough estimate of the eddy

heat flux. On the local scale, thus, the clearest impact of the eddies is the transport of anomalous water masses from the shelf into the deeper waters.

4. Concluding remarks

The conclusions presented here from the time series and accompanying CTD data give a range of insights into the properties, water mass characteristics and transitions of the boundary current in the Arctic Ocean. They are the first attempt to quantify, by direct measurement, the speed, vertical structure and transport of the current, and its partition by the Lomonosov Ridge. Fig. 14 summarizes the transports and suggested pathways discussed above. The results reinforce the picture of Aagaard (1989) of an Arctic Ocean dominated by weak mean flows and strong, isolated eddies. Temperature and salinity data illustrate the leakiness of the ridge, both to deep (1700 m) and shallow (300 m) flows. By capturing the far-reaching effects of changes in the outflow from the Barents Sea, they illustrate the forcing role of the shelves, in particular in maintaining the cold halocline, and the subsequent effect on the Arctic ice cover. The latter suggests a feedback mechanism between ice exported from the Arctic Ocean and ice growth elsewhere.

An appreciation of these features is necessary for an understanding of the Arctic Ocean system, including the communication between the Canadian and Eurasian basins and the influence of the shelves. For example, recent work indicates an increase in the Atlantic influence on the Canadian Basin (e.g., McLaughlin et al., 1996), a situation critically dependent on what waters cross the Lomonosov Ridge. As well as providing a framework for both water mass and tracer studies, these results provide a means of quantifying the validity of the growing array of numerical models of the Arctic.

There are, however, caveats. As many authors note, the 1990s are a time of major change in the Arctic. Indeed, the data presented here support the assumption that variability in the sub-surface layers of the Arctic is predominantly on interannual rather than seasonal timescales. Our results must therefore be viewed in light of a changing Arctic system.

Acknowledgements

We are grateful to Clark Darnall for his meticulous expertise in the mooring work. His dedication, energy and vast skills enriched our personal and professional lives over nearly three decades. We thank also the crew and officers of FS *Polarstern* for their professional assistance at sea; M. Ortmeyer and I. Rigor, Applied Physics Laboratory, for the analysis of the IABP (International Arctic Buoy Programme) data; D. Groves, Applied Physics Laboratory, for the P-E data; J. Blindheim, Marine Research Institute, for the temperature data from Sørkapp; G. Kattner, Alfred-Wegener-Institute, for the nutrient data, and D. Chapman and M. Steele for helpful discussions. This work was funded in part by the Office of Naval Research (grants N00014-99-1-0321 and N00014-96-1-0855), by the Arctic Nuclear Waste Assessment Program, by the National Science Foundation (grant OPP-9504434) and by the Swedish Natural Science Research Council (NFR). This is ESR publication number 23.

Appendix A. Tidal analysis

A record length tidal analysis (Foreman, 1978) is given in Table 3. Like the mean flow, the tidal currents are generally weak, being largest at LM1 and in the surface layers. At LM1, the strongest ($\sim 3\,\mathrm{cm\,s^{-1}}$) tidal component is M_2 at the shallowest instrument ($\sim 100\,\mathrm{m}$), while the S_2 tide is $\sim 2\,\mathrm{cm\,s^{-1}}$. All other components are less than $1\,\mathrm{cm\,s^{-1}}$. At LM2, all components are less than $1\,\mathrm{cm\,s^{-1}}$ at all depths. At LM3, all components are less than $1\,\mathrm{cm\,s^{-1}}$, except at $\sim 100\,\mathrm{m}$, where the M_2 and S_2 components are slightly greater than $1\,\mathrm{cm\,s^{-1}}$.

Appendix B. Extra ice melt in the Barents Sea

From the IABP data, the annual mean speed of ice-transport from summer 1994 to summer 1995 into the Barents Sea increased by $3.5\,\mathrm{cm\,s^{-1}}$ (v_{ice}), compared to the annual mean speed calculated from summer 1993 to 1994, the extra inflow taking place between Spitsbergen and Franz-Joseph Land, a gap some 250 km (G) wide. Assuming a mean ice thickness (I) of 1.5 m (Vinje and Finnekåsa, 1986), over one year (y seconds) an extra $4\times10^{11}\,\mathrm{m^3}$ ($V_{\mathrm{ice}} = v_{\mathrm{ice}}\times G\times I\times y$) of ice was imported into the Barents Sea. Is this volume of ice sufficient to cause the cooling and freshening observed in Section 3.2?

We approach this problem two ways. The first approach is to consider the T–S changes resulting from melting this amount of ice and introducing the melt water directly into the AL in the Arctic Ocean boundary current. By conservation of mass, heat and salt, the resultant salinity is given by

$$\frac{V_{\mathrm{ice}}\rho_{\mathrm{ice}}S_{\mathrm{ice}} + V_{\mathrm{w}}\rho_{\mathrm{w}}S_{\mathrm{w}}}{\rho_{\mathrm{w}}(V_{\mathrm{ice}} + V_{\mathrm{w}})} \sim 34.6\ \mathrm{psu},$$

where ρ_{ice} is the density of the ice ($920\,\mathrm{kg\,m^{-3}}$), ρ_{w} is the density of the water ($1023\,\mathrm{kg\,m^{-3}}$), S_{ice} is the salinity of the ice (4 psu), V_{ice} is the volume of the ice ($4\times10^{11}\,\mathrm{m^3}$), S_{w} is the salinity of the water (34.9 psu, Fig. 8) and V_{w} is the volume of the water ($1.5\ \mathrm{Sv}\times y$, Section 3.2). This is a freshening of the AL by 0.3 psu. The resultant temperature is given by

$$\frac{V_{\mathrm{ice}}\rho_{\mathrm{ice}}c_{\mathrm{ice}}(T_{\mathrm{ice}} - T_{\mathrm{melt}}) + V_{\mathrm{ice}}\rho_{\mathrm{ice}}c_{\mathrm{w}}T_{\mathrm{melt}} + V_{\mathrm{w}}\rho_{\mathrm{w}}c_{\mathrm{w}}T_{\mathrm{w}} - V_{\mathrm{ice}}\rho_{\mathrm{ice}}L_{\mathrm{H}}}{c_{\mathrm{w}}(V_{\mathrm{ice}}\rho_{\mathrm{ice}} + V_{\mathrm{w}}\rho_{\mathrm{w}})} \sim 1.3^{\circ}\mathrm{C},$$

where c_{ice} is the specific heat capacity of ice ($2100\,\mathrm{J\,kg^{-1}\,K^{-1}}$), c_{w} is the specific heat capacity of salt water ($3900\,\mathrm{J\,kg^{-1}\,K^{-1}}$), L_{H} is the latent heat of melting ($333{,}000\,\mathrm{J\,kg^{-1}}$), T_{w} is the initial temperature of the water (2°C, Fig. 8), T_{melt} is the melting temperature of the ice (–1.8°C) and T_{ice} is the initial temperature of the ice (taken as –10°C). This is a cooling of the AL by 0.7°C.

The observed freshening of the AL between 1995 and 1996 ($\sim$ 0.1 psu) could thus be accomplished by melting and injecting about one third of the observed increased ice flux. This would result in a cooling of the AL of $\sim 0.2^{\circ}\mathrm{C}$, which is less than the $\sim 1^{\circ}\mathrm{C}$ cooling observed. The rest of the cooling, $\sim 0.8^{\circ}\mathrm{C}$ (ΔT), could be attributed to atmospheric heat loss, of order $\rho_{\mathrm{w}}Hc_{\mathrm{w}}\Delta T/y \sim 20\,\mathrm{W\,m^{-2}}$ averaged over the year (assuming the thickness of the AL, H, is 200 m). This is well within the observations of heat flux in the area, e.g., Steele and Morison (1993).

Table 3
Summary of tidal components[a]

ID	Lat (N) Lon (E)	Depth (m)		M2			S2			K1			O1			Other components			
		Water	RCM	Ma	Mi	Inc	Ma	Mi	Inc	Ma	Mi	Inc	Ma	Mi	Inc	Name	Ma	Name	Ma
LM1	78°30.8′	1761	106	2.7	−1.6	134	1.9	−1.4	152	0.1	0.0	3	0.1	0.0	85	SSA	1.9	SA	1.6
	133°57.7′		326	0.9	0.1	120	0.7	−0.4	127	0.1	0.0	69	—	—	—	SSA	1.1	MSF	1.0
			761	0.7	0.4	133	0.5	0.0	101	0.1	0.0	65	0.1	0.0	109	MM	0.8	SA	0.8
			1161	0.6	0.5	3	0.6	0.0	56	—	—	—	0.1	0.0	150	SA	1.1	MSF	0.9
LM2	81°4.5′	1721	112	0.5	0.4	38	0.8	−0.5	78	—	—	—	0.1	0.0	53	MM	2.5	SSA	2.0
	138°54.0′		272	0.6	0.2	14	0.8	−0.4	82	0.1	0.0	119	0.1	0.0	46	MM	2.1	SSA	2.1
			712	0.5	0.4	37	0.6	−0.2	56	—	—	—	0.1	0.0	57	MSM	1.2	SA	1.0
			1112	0.5	0.3	35	0.4	0.0	91	0.1	0.0	62	0.1	0.0	75	MSM	0.7	MM	0.5
			1692	0.8	0.1	81	0.9	−0.8	59	0.1	0.0	90	0.1	0.0	21	SA	1.2	MSM	1.1
LM3	80°19.2′	1699	99	1.3	0.4	105	1.0	−0.5	163	0.1	0.1	2	—	—	—	SA	1.8	SSA	1.5
	150°3.5′		269	0.8	0.7	167	0.5	−0.2	151	0.1	0.1	9	—	—	—	SA	1.3	SSA	1.0
			709	0.8	0.4	8	0.2	0.1	43	0.1	0.0	23	—	—	—	SSA	0.8	SA	0.6
			1109	0.8	0.3	3	0.3	0.1	27	0.1	0.1	11	—	—	—	SSA	1.1	SA	0.7

[a] Ma = Semi-major axis, Mi = Semi-minor axis, both in cm s^{-1}. Inc = inclination in degrees. In addition to the M_2, S_2, K_1 and O_1 tides, the remaining two largest components are also quoted, e.g., MSF – lunar fortnightly; MM – lunar monthly; MSM – lunar/solar monthly; SSA – solar semi annual, and SA – solar annual.

The second approach addresses explicitly the mechanism by which ice entering the Barents Sea may melt and enter the AL in the Arctic Ocean boundary current. The additional cold, fresh outflow from the Barents Sea during 1995 to 1996 was estimated in Section 3.2 as $\sim 0.8\,\mathrm{Sv}\,(=Tr)$. Since the main input into the Barents Sea is the warm, salty waters that enter from the Norwegian Sea, this is probably the upstream source of the extra 0.8 Sv. Certainly, taking this warm, salty water (NSW) as the source of the additional cold fresh outflow will give the most extreme test of our hypothesis. We now ask, is the extra ice sufficient to freshen and cool this warm, salty water? Over a year, and assuming an NSW layer thickness of H_b in the Barents Sea, this extra NSW water would occupy an equivalent area (A) of $Tr \times y/H_b$. Dividing the total extra ice (V_{ice}) by this area gives the thickness of ice melted per unit area (H_{ice}), viz.,

$$H_{ice} \sim \frac{V_{ice}}{A} \sim \frac{v_{ice} \times G \times I}{Tr} H_b \sim 0.016 \times H_b,$$

which is $\sim 3.2\,\mathrm{m}$ if $H_b \sim 200\,\mathrm{m}$. (Note this is about twice the estimated ice thickness.) If this ice is melted by and mixed with the NSW, with salinity (S_{nsw}) of 35 psu and temperature (T_{nsw}) of 4°C, the change in salinity (by conservation of salt) will be

$$\frac{\rho_{ice} H_{ice}(S_{nsw} - S_{ice})}{\rho_{ice} H_{ice} + \rho_w H_b} \sim 0.4\,\mathrm{psu},$$

using the values defined above. (Note that H_b cancels out of the expression.) The corresponding change in temperature is given by

$$\frac{\rho_{ice} H_{ice} c_{ice}(T_{melt} - T_{ice}) + \rho_{ice} H_{ice} L_H + \rho_{ice} H_{ice} c_w (T_{nsw} - T_{melt})}{(\rho_{ice} H_{ice} + \rho_w H_b) c_w} \sim 1.3^\circ\mathrm{C}.$$

This would result in a salinity of (35–0.4 psu) ~ 34.6 psu and a water temperature of (4–1.3°C) ~ 2.7°C. The shelf water in the Barents Sea of salinity 34.6 psu is $\sim 3^\circ\mathrm{C}(\Delta T')$ cooler, which implies a heat loss to the atmosphere of $\rho_w H_b c_w \Delta T'$, i.e., $2 \times 10^9\,\mathrm{J\,m^{-2}}$ (assuming H_b is 200 m), equivalent to a heat flux of $\sim 80\,\mathrm{W\,m^{-2}}$ over a year, which is, again, within the observations in the area (e.g., Steele and Morison, 1993).

Thus, the extra ice imported into the Barents Sea between summer 1994 and summer 1995, combined with atmospheric heat loss, can easily account for the cooling and freshening observed in the AL.

Appendix C. CTD sections from Polarstern 1995 cruise

Projected sections of potential temperature (a), salinity (b) and sigma-0 (c), taken in 1995 at the deployment of LM1 (Fig. C1), LM2 (Fig. C2) and LM3 (Fig. C3). The depths and positions of the moored instruments are marked as dots on the sections. Since the true CTD sections do not lie perpendicular to the mean flow, the station separation shown on these plots is obtained by projecting the true positions onto imaginary sections (marked in Fig. 1) which are perpendicular to the local topography (and the mean flow). (Note the bottom topography on the plots is the linear

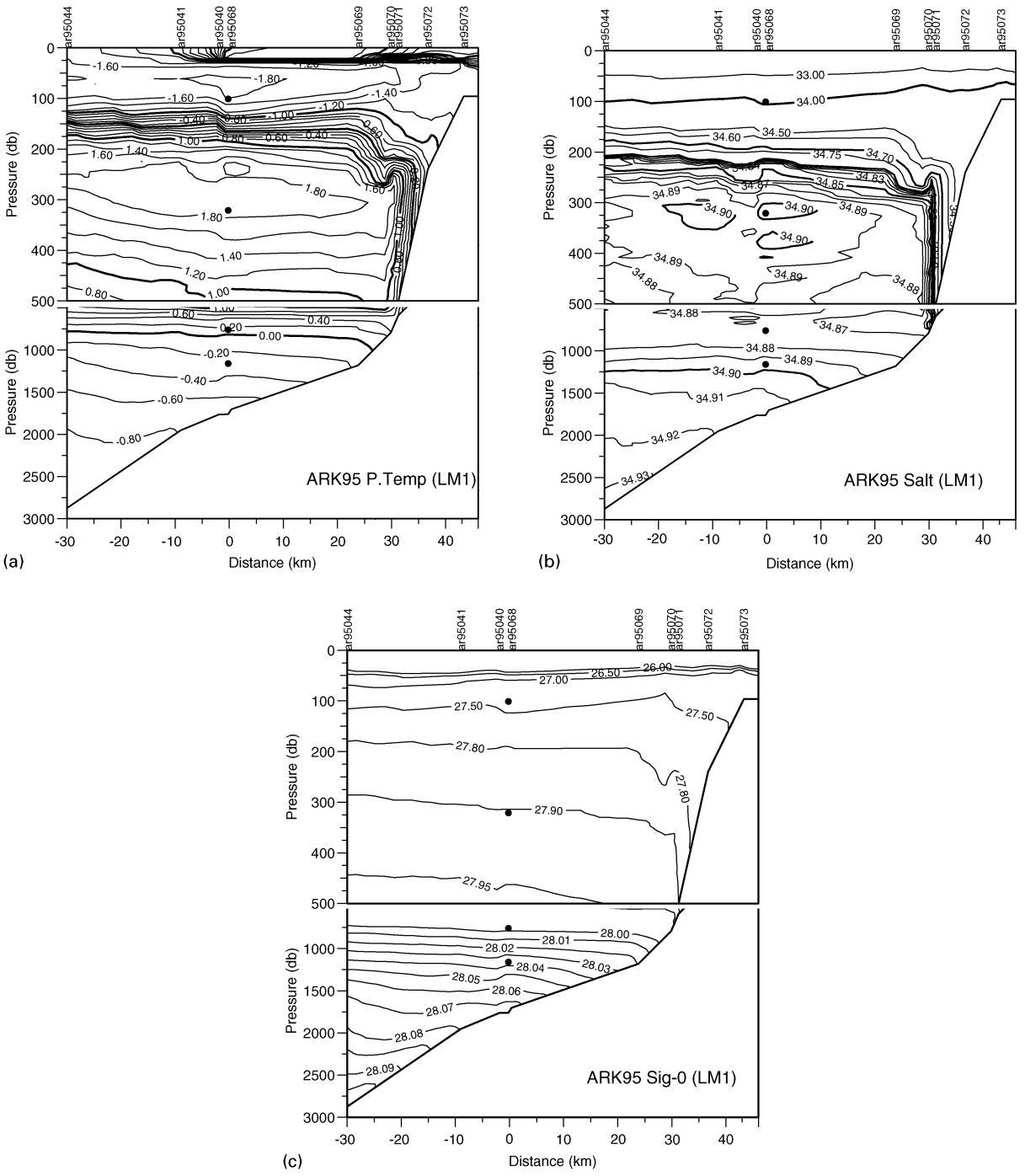
ar95044
ar95041
ar95040
ar95068
ar95069
ar95070
ar95071
ar95072
ar95073
Pressure (db)
Distance (km)
ARK95 P.Temp (LM1)
(a)
ARK95 Salt (LM1)
(b)
ARK95 Sig-0 (LM1)
(c)

Fig. C1.

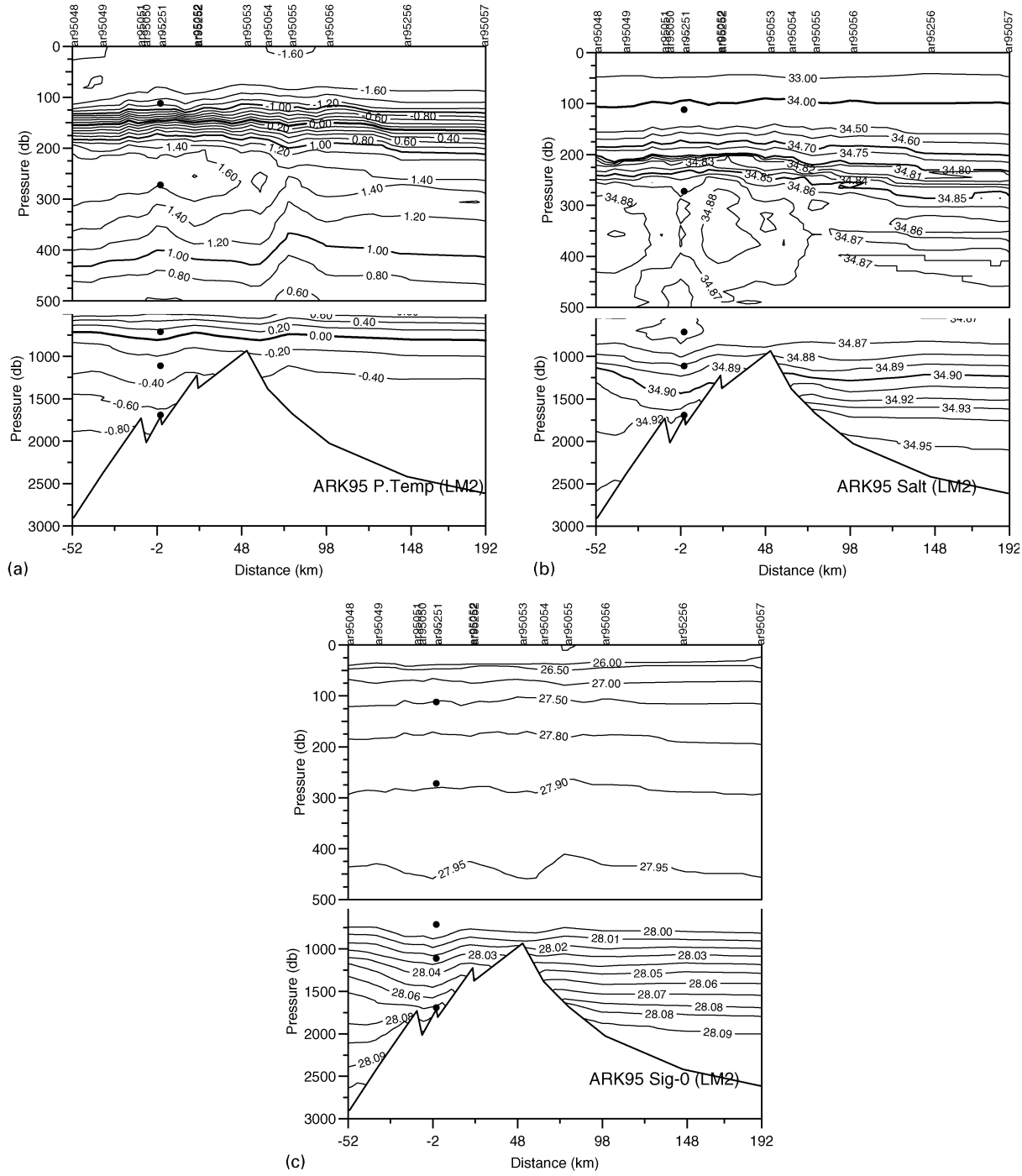
ar95048
ar95049
ar95053
ar95054
ar95055
ar95056
ar95256
ar95057
Pressure (db)
Distance (km)
ARK95 P.Temp (LM2)
ARK95 Salt (LM2)
ARK95 Sig-0 (LM2)
(a)
(b)
(c)

Fig. C2.

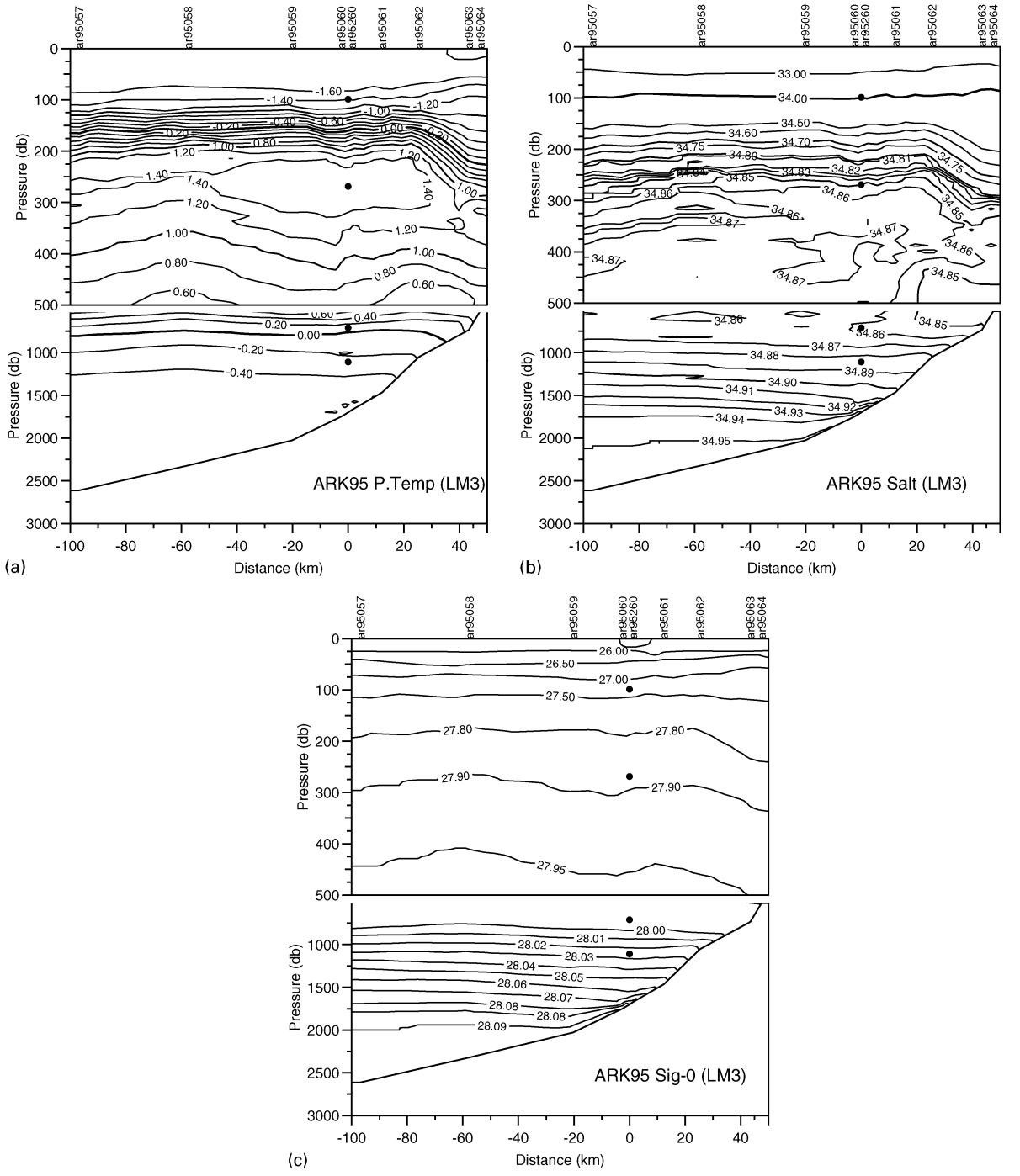
ar95057
ar95058
ar95059
ar95060
ar95260
ar95061
ar95062
ar95063
ar95064
Pressure (db)
Distance (km)
ARK95 P.Temp (LM3)
(a)
ARK95 Salt (LM3)
(b)
ARK95 Sig-0 (LM3)
(c)

Fig. C3.

interpolation of bottom depths of the CTD casts.) Numbers above the plot indicate the individual casts from which the data are interpolated.

References

Aagaard, K., 1981. On the deep circulation in the Arctic Ocean. Deep-Sea Research 28, 251–268.

Aagaard, K., 1989. A synthesis of the Arctic Ocean circulation. Rapp. P.-V. Reun. Cons. Int. Exploration de la Mer 188, 11–22.

Aagaard, K., Coachman, L.K., Carmack, E., 1981. On the halocline of the Arctic Ocean. Deep-Sea Research 28A (6), 529–545.

Aagaard, K., Swift, J.H., Carmack, E.C., 1985. Thermohaline circulation in the Arctic Mediterranean seas. Journal of Geophysical Research 90 (C3), 4833–4846.

Anderson, L.G., Björk, G., Holby, O., Jones, E.P., Kattner, G., Koltermann, K.P., Liljeblad, B., Lingegren, R., Rudels, B., Swift, J., 1994. Water masses and circulation in the Eurasian Basin: results from the Oden 91 expedition. Journal of Geophysical Research 99 (C2), 3273–3283.

Augstein, E., The Cruise Participants. 1997. The expedition ARCTIC'96 of RV Polarstern (ARKXII) with the Arctic Climate System Study (ACSYS) Vol 234. Bericht zur Polarforschung, Alfred-Wegener-Institute, Bremerhaven, Germany, 54pp. (unpublished manuscript).

Blindheim, J., Borovkov, V., Hansen, B., Malmberg, S.-Aa., Turrell, W.R., Østerhus, S., 2000. Upper layer cooling and freshening in the Norwegian Sea in relation to atmospheric forcing. Deep-Sea Research I 47, 655–680.

Boyd, T., Moustafa, M.S., Steele, M., 1997. Submarine-based hydrographic observations of the Arctic Ocean: March–May 1995: SCICEX-95. Oregon State Univ. Data Report 165, Ref. 97-3 88pp. (unpublished manuscript).

Chapman, D.C., 1999. Dense water formation beneath a time-dependent coastal polynya. Journal of Physical Oceanography 29, 807–820.

Coakley, B.J., Edwards, M.H., Chayes, D., Okkonen, S., Rognstad, M.R., Stockwell, D., Whitledge, T.E., 1999. Arctic Basin insights 2: new data for the Eurasian Basin and Lomonosov Ridge from SCICEX-99. EOS 80, F993–F994.

D'Asaro, E.A., 1988. Observations of small eddies in the Beaufort Sea. Journal of Geophysical Research 93 (C6), 6669–6684.

Dewey, R., Muench, R., Gunn, J., 1999. Mixing and vertical heat flux estimates in the Arctic Eurasian Basin. Journal of Marine Systems 21, 199–205.

Foldvik, A., Aagaard, K., Tørresen, T., 1988. On the velocity field of the East Greenland Current. Deep-Sea Research 35 (8), 1335–1354.

Foreman, M.G.G., 1978. Manual for tidal currents analysis and prediction. Pacific Marine Science Report 78-6, Institute of Ocean Sciences, Patricia Bay, Victoria, B.C., 70pp, unpublished manuscript.

Frank, M., Smethie Jr., W.M., Bayer, R., 1998. Investigation of subsurface water flow along the continental margin of the Eurasian Basin using the transient tracers tritium, ^{3}He, and CFCs. Journal of Geophysical Research 103 (C13), 30773–30792.

Gill, A.E., 1982. Atmosphere-Ocean Dynamics. Academic Press, Inc., New York, 662pp.

Gorshkov, S.G., 1983. World Ocean Atlas. Volume 3: Arctic Ocean. Pergamon Press, Oxford.

Hanzlick, D.J., 1983. The West Spitsbergen Current: transport, forcing, and variability. Ph.D. Dissertation, Sch.Oceanogr., Uni.Wash., Seattle, 127pp.

HDNO-Head Dept of Navigation and Oceanography; Russian Ministry of Defence and VNIIOkeangeologiya (All Russia Institute for Geology and Mineral Resources of the World Ocean; Russian Academy of Sciences.), 1999. Bottom Relief of the Arctic Ocean. St. Petersburg, Russia.

Holloway, G., 1987. Systematic forcing of large-scale geophysical flows by eddy-topography interaction. Journal of Fluid Mechanics 184, 463–476.

Hunkins, K., 1966. Ekman drift currents in the Arctic Ocean. Deep-Sea Research 13, 607–620.

Jones, E.P., Rudels, B., Anderson, L.G., 1995. Deep waters of the Arctic Ocean: origins and circulation. Deep-Sea Research I 42, 737–760.

Jónsson, S., 1989. The structure and forcing of the large- and mesoscale circulation in the Nordic seas, with special reference to the Fram Strait. Ph.D. Dissertation, Uni.Bergen, 144pp.

Jungclaus, J.H., 1999. A three-dimensional simulation of the formation of anticyclonic lenses (Meddies) by the instability of an intermediate depth boundary current. Journal of Physical Oceanography 29, 1579–1598.

Killworth, P.D., 1980. Barotropic and baroclinic instability in rotating stratified fluids. Dynamics of Atmospheres and Oceans 4, 143–184.

Killworth, P.D., 1992. An equivalent-barotropic mode in FRAM. Journal of Physical Oceanography 22 (11), 1379–1387.

Loeng, H., Ozhigin, V., Ådlandsvik, B., Sagen, H., 1993. Current measurements in the northeastern Barents Sea. Ices Statutory Meeting 1993, C.M.1993 C:41, 22pp.

Manley, T.O., Hunkins, K.L., 1985. Mesoscale eddies of the Arctic Ocean. Journal of Geophysical Research 90 (C3), 4911–4930.

McLaughlin, F.A., Carmack, E.C., Macdonald, R.W., Bishop, J.K.B., 1996. Physical and geochemical properties across the Atlantic/Pacific water mass front in the southern Canadian Basin. Journal of Geophysical Research 101, 1183–1197.

McPhee, M.G., Smith, J.D., 1976. Measurements of the turbulent boundary layer under pack ice. Journal of Physical Oceanography 6, 696–711.

Mysak, L.A., Muench, R.D., Schumacher, J.D., 1981. Baroclinic instability in a downstream varying channel: Shelikof Strait, Alaska. Journal of Physical Oceanography 11, 950–969.

Nansen, F., 1902. The oceanography of the North Polar Basin. Norwegian North Polar Expedition, 1893–1896, Scientific Results V (IX), 427pp.

Nazarenko, L., Holloway, G., Tausnev, N., 1998. Dynamics of transport of "Atlantic signature" in the Arctic Ocean. Journal of Geophysical Research 103 (C13), 31003–31015.

Newton, J.L., Aagaard, K., Coachman, L.K., 1974. Baroclinic eddies in the Arctic Ocean. Deep-Sea Research 21, 707–719.

Overland, J.E., Colony, R.L., 1994. Geostrophic drag coefficients for the central Arctic derived from Soviet drifting station data. Tellus 46A, 75–85.

Perry, R.K., Fleming, H.S., 1986. Bathymetry of the Arctic Ocean. Naval Research Laboratory, Washington, D.C.20375.

Rudels, B., Anderson, L.G., Jones, E.P., 1996. Formation and evolution of the surface mixed layer and halocline of the Arctic Ocean. Journal of Geophysical Research 101 (C4), 8807–8821.

Rudels, B., Jones, E.P., Anderson, L.G., Kattner, G., 1994. On the origin and circulation of the Atlantic layer and intermediate depth waters in the Arctic Ocean. In: Johannessen, O.M., Muench, R.D., Overland, J.E. (Eds.), The Polar Oceans and Their Role in Shaping the Global Environment, Geophysical Monograph Series, Vol. 85. AGU, Washington, DC, pp. 33–46.

Rudels, B., Meyer, R., Fahrbach, E., Ivanov, V., Østerhus, S., Quadfasel, D., Schauer, U., Tverberg, V., Woodgate, R.A., 2000a. Water mass distribution in Fram Strait and over the Yermak Plateau in summer 1997. Annales Geophysicae 18(6), 687–705.

Rudels, B., Muench, R.D., Gunn, J., Schauer, U., Friedrich, H.J., 2000b. Evolution of the Arctic Ocean Boundary Current north of the Siberian Shelves. Journal of Marine Systems 25, 77–99.

Schauer, U., Muench, R.D., Rudels, B., Timokhov, L., 1997. Impact of eastern Arctic shelf waters on the Nansen Basin intermediate layers. Journal of Geophysical Research 102 (C2), 3371–3382.

Steele, M., Boyd, T., 1998. Retreat of the cold halocline layer in the Arctic Ocean. Journal of Geophysical Research 103, 10419–10435.

Steele, M., Morison, J.H., 1993. Hydrography and vertical fluxes of heat and salt northeast of Svalbard in autumn. Journal of Geophysical Research 98 (C6), 10013–10024.

Swift, J.H., Jones, E.P., Aagaard, K., Carmack, E.C., Hingston, M., Macdonald, R.W., McLaughlin, F.A., Perkins, R.G., 1997. Waters of the Makarov and Canada basins. Deep-Sea Research 44 (8), 1503–1529.

Swift, J.H., Takahashi, T., Livingston, H.D., 1983. The contribution of the Greenland and Barents seas to the deep water of the Arctic Ocean. Journal of Geophysical Research 88 (C10), 5981–5986.

Vinje, T., Finnekåsa, Ø., 1986. The ice transport through the Fram Strait. Norsk-PolarInstitutt Skrifter 186, 39pp.

Woodgate, R.A., Schauer, U., Fahrbach. E., 1998. Moored current meters in the Fram Strait at 79°N: preliminary results with special emphasis on the West Spitsbergen Current. Bericht aus dem Fachbereich Physik, Alfred-Wegener-Institute, Bremerhaven, Germany, 91, 170pp. (unpublished manuscript).

Worthington, L.V., 1953. Oceanographic results of Project SKIJUMP I and SKIJUMP II in the Polar Sea, 1951–1952. Transactions, AGU 34 (4), 543–551.